CONSTRAINING THE INTERPRETATION OF AVOA FOR FRACTURE CHARACTERISATION

Stephen A. Hall[*,†] **and J-Michael Kendall**[*]

[*]*School of Earth Sciences, University of Leeds, Woodhouse Lane, Leeds, LS2 9JT, UK.*
[†]*Now at Department of Petroleum Engineering, Heriot-Watt University, Edinburgh, EH14 4AS, UK.*

Abstract. This paper investigates the use of seismic anisotropy and amplitude variation with offset and azimuth (AVOA) for fracture characterisation. Specifically the aim of this work is to provide links between rock and fracture properties, elastic modelling and the interpretation of seismic signatures to reduce the potential ambiguity when interpreting AVOA data. Analytical expressions and numerical modelling are used to highlight the sensitivity of AVOA to fracture properties. Furthermore, little prior attention has been paid to wave propagation in media with multiple fracture alignments or fractured media with a permeable matrix therefore an investigation of AVOA for these cases is included. P-wave AVOA is of obvious interest since there are more of these data. However converted wave and shear-wave AVOA are also investigated as these may provide additional insight into fracture characteristics. It is shown that P-P and P-S AVOA hold significant information about fracturing but potential ambiguity in the interpretation of these data is observed that could lead to incorrect determination of fracture orientation. This highlights the need for forward modelling with rock properties data to constrain the interpretation. Additionally, shear-wave (S-S) AVOA is shown to exhibit significant azimuthal variations which provide strong indications of fracture orientation but only at near offsets and little insight can be gained into other fracture properties.

1 Introduction

The presence of aligned fracturing can cause a medium to exhibit elastic anisotropy. Therefore observations of variations in seismic attributes, such as traveltimes, velocities or reflection amplitudes, can provide insight into the properties of fractures which are below the resolution of standard seismic techniques. Such information may be utilized to improve production in many hydrocarbon reservoirs by, for example, optimizing horizontal drilling and water floods.

Fracture characterization using seismic anisotropy has been previously demonstrated through a variety of methods. For example, Crampin and Lovell (1991) and Potters et. al. (1999) use shear-wave splitting to characterize aligned fractures. Azimuthal variations in seismic velocities and traveltimes have also been shown to provide insight into subsurface fracturing (e.g., Crampin et al., 1986; Li, 1997; Horne et al. 1997). Mueller (1991) and Kendall and Kendall (1996) observe direct correlations between shear-wave amplitude anomalies and areas of high hydrocarbon production attributed to aligned fracturing. Amplitude variation with offset (AVO) (see, for example, Castagna and Backus, 1993) has for a long time been recognized as a useful indicator of lithology (e.g., Ostrander, 1984; Rutherford and Williams, 1980) and pore fill (e.g., Castagna and Swan, 1997). More recently, the analysis of P-wave amplitude variation with offset and azimuth (AVOA) has been utilised for fracture characterization (e.g., Thomsen, 1988; Lynn et al. 1995;

Anisotropy 2000: Fractures, converted waves and case studies
Published by
The Society of Exploration Geophysicists
P.O.Box 702740, Tulsa, OK 74170-2740

Harwood et al., 1998; Mallick et al., 1908; Macbeth et al., 1999; Hall and Kendall, 1999; Hall et al., 2000a). This paper investigates the effects of aligned fracturing on seismic reflectivity using numerical modeling and analytical analysis. The advantage of considering reflection amplitudes, over traveltime and velocity methods, is that it is not necessary to have significant lithological thickness to detect azimuthal variations in data. Thus AVOA provides good vertical resolution and characterizes azimuthal attributes local to the reflector of interest. By contrast, traveltime or velocity analysis show an accumulated effect through overlying layers.

To interpret anisotropy in seismic data for fracture characterization, it is first necessary to understand how the nature of the fracturing relates to the observations. Thus this work investigates the influence of aligned fracturing on variations, with angle and azimuth of incidence, of seismic reflection at an interface between anisotropic fractured media. First, the general reflection/transmission problem in anisotropic media is briefly reviewed, followed by the introduction of AVOA in media containing aligned vertical fractures using simplified equations for P-P AVOA. Following this overview, numerical modelling provides insight into the sensitivity of P-P, P-S and S-S AVOA to the properties of vertically aligned fractures. A more detailed investigation of P-P AVOA, using analytical equations, is subsequently given, since these data have been of significant recent interest (e.g., *Geophysics* special issue on P-wave anisotropy, 1999).

There has been recent interest in how the response of fractures to an applied stress is modified if fluid may flow from fractures to the surrounding matrix porosity in the time scale of a seismic wave (e.g., Thomsen, 1995; Hudson et al., 1996). Therefore, the modeling and analysis in this paper, which first considers isolated fractures, are extended to take into account the hydraulic connectivity of fractures and *equant* matrix porosity. Furthermore, the case of a single alignment of fracture orientations with or without equant porosity is extended to consider multiple fracture alignments, since this is the more likely natural state. This provides insight into the expected AVOA signatures from multiple fracture sets and how this may change with the preferential closure of different fracture sets such as may result from changes in stress fields (e.g., during production).

This paper pays particular attention to P-waves, as there are obviously more of these data already in use. In addition, they are relatively cheap to acquire and easier to process in comparison to shear-wave or converted wave data. Furthermore, P-wave AVOA has recently been of great interest in oil and gas exploration (e.g., Hall et al. 2000). Nevertheless, other phases, e.g., shear-waves and converted waves (produced by phase conversion on reflection or transmission at an interface) are also treated, as these data are now becoming more commonly considered due to recent advances in processing and acquisition technology (i.e., 4C ocean bottom acquisition). These data may hold significant complementary information about fracture properties, so the potential for their use in fracture characterization is discussed. The main questions that are to be investigated in this paper can be summarized as follows. Are P-wave data alone capable of characterizing fracturing? What additional information can be gained from shear and converted phases? How will multiple fracture alignments affect the interpretation of data? How will hydraulic connectivity of fractures and pore-space affect AVOA properties?

2 AVOA in anisotropic, fractured media

The reflectivity of an interface depends on the slownesses (and therefore the phase velocities) parallel to the reflecting interface. As velocities vary with azimuth in fractured media, it is therefore clear that AVO will depend on fracture characteristics and vary azimuthally. This section investigates reflection coefficients in anisotropic fractured media. The

azimuthal variation in P-P reflection is investigated in more detail. However, numerical modeling in the following sections includes shear and converted phases in order to assess their usefulness in AVOA analysis for fracture characterization.

Reflection from an interface between isotropic media is relatively simple, with coupled P and S_v waves producing secondary P and S_v waves only and incident S_h waves being reflected or refracted as just S_h waves. Exact reflection and transmission coefficients for plane waves at a boundary between two isotropic half-spaces are provided by Aki and Richards (1980). However, data analysis usually employs simplifications of the exact solution such as those provided by Chapman (1976) and Shuey (1985) for P-P reflection, which have the general form

$$R_{pp}(i) = A + B\sin^2 i + C\sin^2 i\tan^2 i \qquad (1)$$

for an incidence phase angle *i*. The terms *A*, *B* and *C* are defined by Chapman(1976) as

$$\begin{aligned} A &= \frac{1}{2}\left[\frac{\Delta Z}{\overline{Z}}\right], \\ B &= \frac{1}{2}\left[\frac{\Delta\alpha}{\overline{\alpha}} - \left(\frac{2\overline{\beta}}{\overline{\alpha}}\right)^2 \frac{\Delta G}{\overline{G}}\right], \\ C &= \frac{1}{2}\left[\frac{\Delta\alpha}{\overline{\alpha}}\right]. \end{aligned} \qquad (2)$$

Here $Z = \rho\alpha$ is the P-wave impedance and $G = \rho\beta^2$ is the shear modulus where α, β and ρ are, respectively, the P-wave velocity, shear-wave velocity and density. The symbol Δ indicates differential values. For example, $\Delta\alpha = \alpha_2 - \alpha_1$, and the over-scored terms are the average values, e.g. $\overline{\alpha} = (\alpha_2 + \alpha_1)/2$, where the subscripts, 1 and 2, indicate the properties of the upper and lower bounding media, respectively.

The extension of the reflection and transmission problem to include anisotropy requires an understanding of the anisotropic elasticity of the bounding media and slownesses of the propagating waves. For horizontally layered (VTI) media this extension is relatively straightforward, as the horizontal slownesses and elasticity do not change with direction, so, as with the isotropic case, there are coupled P and S_v phases uncoupled from the S_h waves (see, for example, Thomsen, 1993). When azimuthal anisotropy exists (e.g., in a vertically fractured medium) the reflection coefficients will have a dependence on both the angle and azimuth of incidence, so the problem is now in three dimensions. Furthermore, the energy of a wave incident at such an interface is partitioned between six possible secondary waves (three reflected and three transmitted; see Figure 1). To demonstrate the nature of AVOA in azimuthally anisotropic media, the case of P-P reflectivity from a layer with a single set of aligned fractures is discussed using simplified equations. The derivation of a general method for calculating exact reflection coefficients in anisotropic media (used in the numerical modeling of this paper) is outlined by Guest (1998) and Guest et al. (1993), so here an exhaustive review is omitted.

Equation 1 presented the general form for P-P AVO in azimuthally isotropic media. However, as discussed above, if either of the media bounding the interface is azimuthally anisotropic, the AVO will have an azimuthal dependence. Rüger (1998) and Vavryčuk and Pšenčík (1998) extend the basic AVO approximation (equation 1) to provide analytical equations describing P-wave AVOA in media with a single fracture alignment. Thus the P-P reflection amplitude, R_{pp}, may be given (after Rüger, 1998) as a function of the incident and azimuthal phase angles, *i* and ϕ, respectively:

$$\begin{aligned} R_{pp}(i,\phi) = A + [B + D\cos 2(\phi)\,]\sin^2 i + \\ [C + E\cos 2(\phi) + F\cos 4(\phi)] \\ \sin^2 i\tan^2 i, \end{aligned} \qquad (3)$$

where *A, B, C, D, E* and *F* are functions of the contrasts in velocity and azimuthal anisotropy parame-

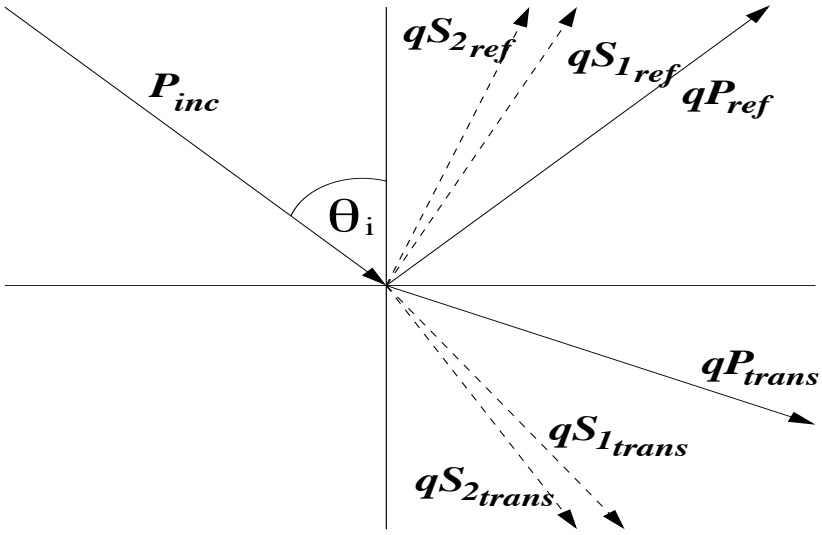

Figure 1: *Energy partitioning at an interface in anisotropic media for an incident P-wave. Energy partitioning at an interface in anisotropic media for an incident P-wave. Three reflected (ref) and three transmitted (trans) phases are generated at an interface in anisotropic media. Here a P-wave is incident at the reflector with angle θ_i and P- and S-waves are reflected and transmitted (dashed lines indicate S-waves) with the q indicating that these are not pure compressional or shear modes. Note that for an isotropic-anisotropic interface there will only be a single reflected shear-wave but this will have both horizontal and vertical components to its displacement.*

ters across the reflecting interface

$$
\begin{aligned}
A &= \frac{1}{2}\frac{\Delta Z}{\overline{Z}}, \\
B &= \frac{1}{2}\left[\frac{\Delta\alpha}{\overline{\alpha}} - \left(\frac{2\overline{\beta}}{\overline{\alpha}}\right)^2 \frac{\Delta G}{\overline{G}} + \Delta\delta^{(v)} + \right. \\
&\qquad \left. 2\left(\frac{2\overline{\beta}}{\overline{\alpha}}\right)^2 \Delta\gamma\right], \\
C &= \frac{1}{2}\frac{\Delta\alpha}{\overline{\alpha}} + \frac{1}{8}(3\Delta\epsilon^{(v)} + 2\Delta\delta^{(v)}), \\
D &= \frac{1}{2}\left[\Delta\delta^{(v)} + 2\left(\frac{2\overline{\beta}}{\overline{\alpha}}\right)^2 \Delta\gamma\right], \\
E &= \frac{1}{2}\Delta\epsilon^{(v)}, \\
F &= \frac{1}{8}\left[\Delta\epsilon^{(v)} - 2\Delta\delta^{(v)}\right].
\end{aligned}
\tag{4}
$$

Here $Z = \rho\alpha$ and $G = \rho\beta^2$ are now the vertical P-wave impedance and shear modulus for the vertical (fracture parallel) P-wave and the shear-wave velocities, α and β, respectively, and density, ρ. The parameters $\epsilon^{(v)}$ and $\delta^{(v)}$ are the alternative Thomsen parameters used by Rüger (1998) to study HTI media, defined as

$$
\begin{aligned}
\epsilon^{(v)} &= \frac{C_{11} - C_{33}}{2C_{33}} \\
&\equiv -\frac{\epsilon^r}{1 + 2\epsilon^r}, \\
\delta^{(v)} &= \frac{(C_{13} + C_{66})^2 - (C_{33} - C_{66})^2}{2C_{33}(C_{33} - C_{66})} \\
&\equiv \frac{\delta^r - 2\epsilon^r(1 + \epsilon^r/f)}{(1 + 2\epsilon^r)(1 + 2\epsilon^r/f)},
\end{aligned}
\tag{5}
$$

where the terms ϵ^r and δ^r are the rotated Thomsen parameters defined in Appendix A. The function f is defined as $f = 1 - v_{s_0}/v_{p_0}$, where v_{p_0} and v_{s_0} are the velocities perpendicular to fracturing. Rüger (1998) uses the same definition of γ as Thomsen (1995).

From equation (3), it can be seen that the P-P AVO will vary with azimuth by a combination of $\cos 2\phi$

and $\cos 4\phi$ components. However, many previous studies have been based on the assumption of only a $\cos 2\phi$ (elliptical) azimuth dependence in AVO (e.g., Mallick et al., 1998). At near offsets only the $\sin^2 i$ terms, in equation (3), will be significant since at these offsets $\tan^2 i$ is small. This suggests that at near offsets the assumption of a $\cos 2\phi$ variation in AVO with azimuth may be valid. For longer offsets the magnitude of $\tan^2 i$ increases, so the variation with $\cos 4\phi$ will be increased and the azimuthal trend may no longer be elliptical. Thus for longer offsets the assumption of ellipticity may not be valid and could lead to erroneous conclusions. Furthermore, the sign of *D*, describing the elliptical near-offset azimuthal variation in the AVO, can be positive or negative, as can that of the isotropic AVO gradient *B*. This means that the direction of the maximum AVO gradient does not necessarily coincide with the fracture strike orientation, as often assumed (e.g., Mallick et al., 1998), and may lead to confusion in interpretation.

From the discussion above it is clear that there may be ambiguity in the interpretation of AVOA in terms of fracture characteristics and orientation. The following section presents numerical modeling to gain insight into how reflection amplitudes vary with offset and azimuth in media with fracture-induced seismic anisotropy. In addition to P-P AVOA, P-S and S-S reflections are also presented in order to investigate how these data may be utilized in fracture characterization. Following this modeling, further analysis of P-P AVOA is provided in order to quantify some of the observations and to provide insight into how AVOA data may be used for fracture characterization.

3 Numerical modeling of AVOA in media containing vertical fractures

In this section, calculated reflection coefficients are used to assess the sensitivity of AVOA to changes in fracture parameters. The reflection coefficients are calculated using the FORTRAN program REFVEC (Guest and Kendall, 1993), which is based on the theory outlined in Guest (1993) and Guest et al. (1998). Plots of AVO and AVAz (amplitude variation with azimuth) show the *total displacement ratio* for the incident versus reflected wave amplitudes as a function of incidence angle or azimuth. Fracture-induced anisotropy is modeled using the EFFECH approach (Hall, 2000, see Appendix B) to investigate the change in AVOA due to variations in the fracture aspect ratio (*d*) and crack density (η_c). The model comprises an isotropic shale ($v_p = 2738ms^{-1}, v_s = 1110ms^{-1}$ and $\rho = 2690kgm^{-3}$) overlying a fractured chalk ($v_p = 4000ms^{-1}, v_s = 1740ms^{-1}$ and $\rho = 3180kgm^{-3}$) with a gas or brine fracture fill. P-P, P-S and S-S phases are compared to assess the relative merits of each phase for fracture characterization. The P-S phase considered here is the P-qS$_v$ conversion at the reflecting interface. In a marine environment the S-S reflection results from P-S$_v$ conversion on transmission at the sea floor.

A P-wave or S_v-wave incident at a boundary in anisotropic media will be reflected as a P-wave and two shear waves (see Figure 1). In the model used here, the overlying medium is isotropic, so only a single shear wave will be reflected. However, due to the anisotropy of the lower medium, the reflected shear wave will not be a pure S_v- or S_h-wave. This shear wave will have both horizontal and vertical components of displacement, with magnitudes indicated by the reflected S_h and S_v displacement ratios. The S_h displacement will lead to a nonzero amplitude on the transverse component of multicomponent seismic data, and the S_v will contribute to the radial and vertical records.

The AVOA for incident P- and S_v-waves are plotted in Figures 2 and 3 for $\eta_c = 0.1$ and $d = 0.001$ and a brine or gas fill, respectively. From these figures it is clear that significant azimuthal variation in the P-P and P-S_v reflection amplitudes will be observed only at longer offsets, near to the P-wave

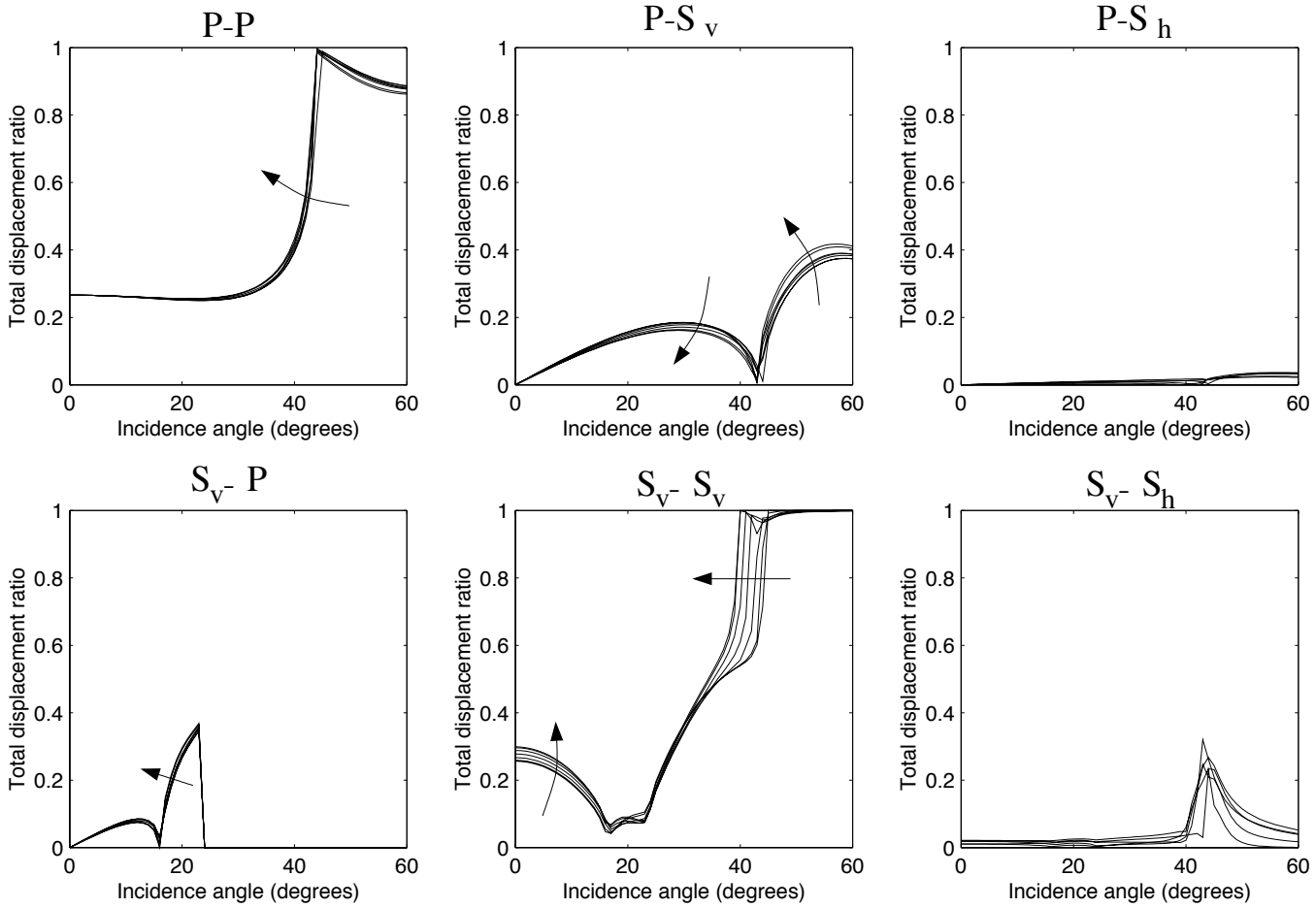

Figure 2: *AVO curves for incident P and S_v at different for aligned brine-filled fractures. AVO curves for incident P and S_v and all possible reflection phases at $0^o, 15^o, 30^o, 45^o, 60^o$ and 90^o azimuth relative to the fracture normal direction (arrows indicate increasing azimuth) for aligned brine-filled fractures with d=0.001 and $\eta_c = 0.1$. Note that S_v and S_h refer to the vertical and horizontal components of a single reflected shear-wave.*

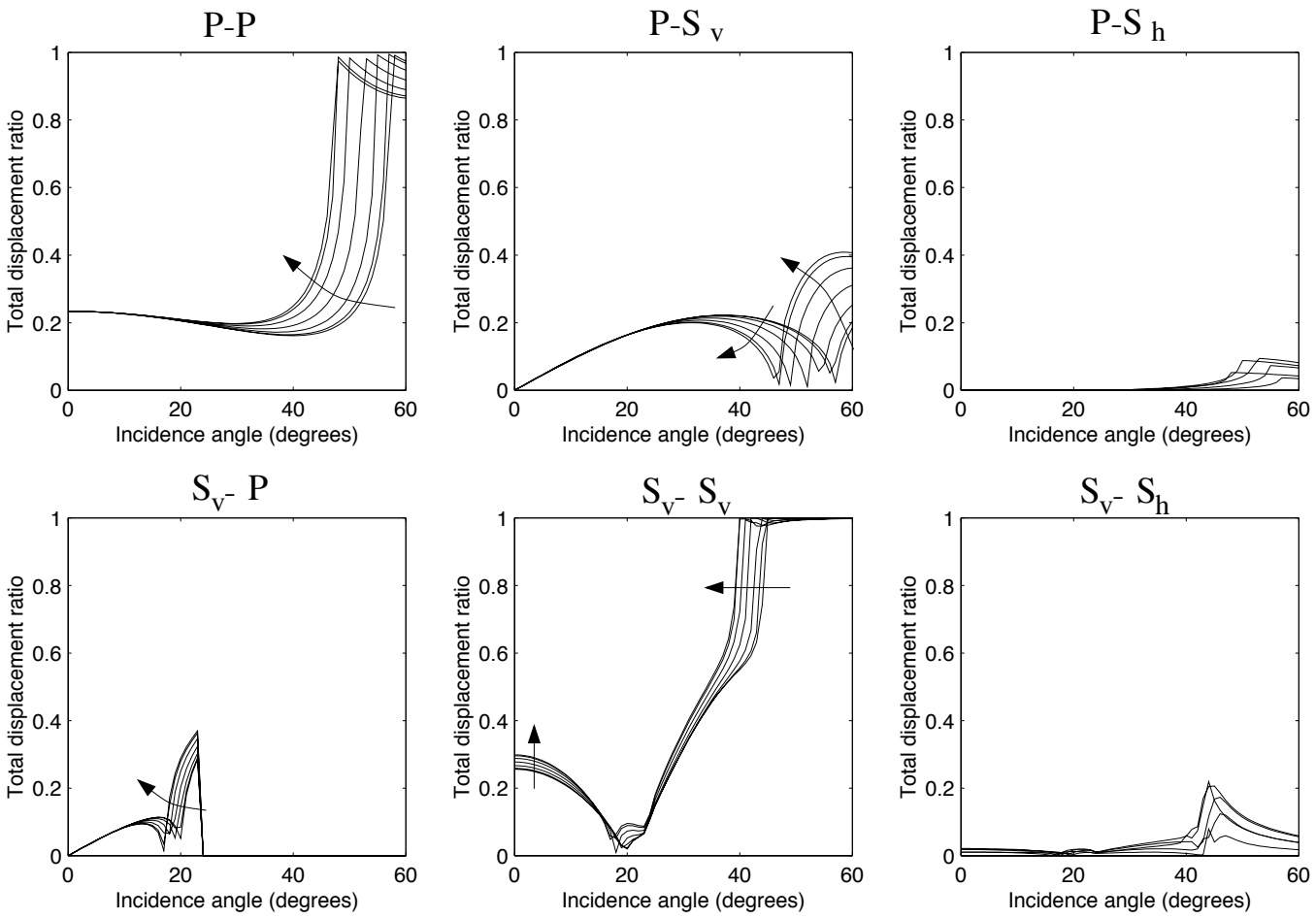

Figure 3: *AVO curves for incident P and S_v at different for aligned gas-filled fractures. AVO curves for incident P and S_v and all possible reflection phases at $0^o, 15^o, 30^o, 45^o, 60^o$ and 90^o azimuth relative to the fracture normal direction (arrows indicate increasing azimuth) for aligned gas-filled fractures with d=0.001 and $\eta_c = 0.1$. Note that S_v and S_h refer to the vertical and horizontal components of a single reflected shear-wave.*

critical reflection angle (marked by the peak in reflection amplitude). However, both phases appear to show greater azimuthal variations for gas-filled fractures than for a brine fill. It should be noted that this conclusion is dependent on the particular model or the offsets being considered and later sections show cases where the opposite is true. At short offsets the S_v-S_v AVO shows significant variability with azimuth but little difference between a brine and a gas fracture-fill. Other significant features, highlighted by Figures 2 and 3, that could be used for fracture characterization are (i) variations in the onset of the P-P critical reflection, (ii) changes in the angle at which the shear-wave reflections switches polarity and (iii) the presence of energy on the transverse component (i.e., nonzero S_h reflection amplitude). The P-P critical angle, θ_{c_p}, is indicated by the sharp peak in amplitude around 40^o to 50^o and occurs at shorter incidence angles as the azimuth of incidence moves away from the fracture normal. A similar trend is observed for the angle at which the S_v component changes polarity (appearing on the plots as a decrease to zero in the P-S_v reflection amplitude, followed by an immediate, abrupt increase). Transverse energy will be recorded only along azimuths oblique to the fracture-strike and fracture-normal directions where the S_h component is coupled with the P- and S_v components. All of these features may be clear indicators of anisotropy, although 3D structure can also produce similar effects.

Figures 4-7 show the P-P, P-S and S_v-S AVAz for a range of fracture parameters and three fixed incidence angles. For an incident P-wave, three incidence angles below the P-P critical reflection angle are considered: $20^o, 30^o$ and 40^o (θ_{c_p} is around 50^o). For an incident S_v-wave, incidence angles of $0^o, 7.5^o$ and 15^o are considered, since significant variations are seen at short offsets for these phases and to avoid complex amplitudes, which will occur after the onset of the first shear-wave critical reflection angle at around 20^o. The first general observation from these plots is that the azimuthal variations in reflection amplitudes have 90^o and 180^o periodicities. These periodicities have the form of $\cos 4\phi$ and $\cos 2\phi$, respectively, as described in equation (3). Furthermore, the $\cos 2\phi$ trend is seen to be positive or negative, with respect to the azimuth from the fracture-normal direction.

Figure 4 shows the dependence of the AVAz on the aspect ratio of brine-filled fractures. At near offsets (up to about 30^o) the P-P reflection shows a positive $\cos 2\phi$ trend when the aspect ratio is very small (around 0.0001) and a negative $\cos 2\phi$ trend with a higher aspect ratio. When the incidence angle is greater than about 30^o, there is a $\cos 4\phi$ dependence with low aspect ratios, but for aspect ratios higher than about 0.01, a negative $\cos 2\phi$ trend dominates. For all offsets, decreasing the aspect ratio reduces the volume fraction of the low-velocity fractures, so the aggregate velocity is higher and the overall reflection amplitude is increased. The P-S_v phase has a negative $\cos 2\phi$ dependence for low aspect ratio, at short offsets, and a $\cos 4\phi$ azimuthal variation as the incidence angle increases. Larger aspect ratios provide a positive $\cos 2\phi$ trend. The S_v-S_v reflection shows significant azimuthal variations for a vertically incident wave, although in a marine survey it is unlikely that it would be possible to acquire such incidence angles. However, the short-offset data are viable, and these show a simple negative $\cos 2\phi$ dependence, which has little dependence on aspect ratio until around 15^o incidence, where a $\cos 4\phi$ component influences the AVOA signature. With a gas fracture-fill, Figure 5, trends very similar to those described for a brine fill are seen. However, the range of aspect ratio used is much lower than in Figure 4, and the $\cos 2\phi$ variation in P-P reflection is only observed at 40^o and with an aspect ratio lower than 0.0001 (compared to about 0.01 for a brine-fill).

In Figure 6 the variations of AVAz with crack density are presented. For all phases AVAz has very little sensitivity to the crack density term for brine-filled fractures. For gas-filled fractures (Figure 7) there is a significant change in the AVAz with crack density, but this is mainly a change in magnitude of the azimuthal anisotropy and not a change in symmetry. This effect is due to a large influence on

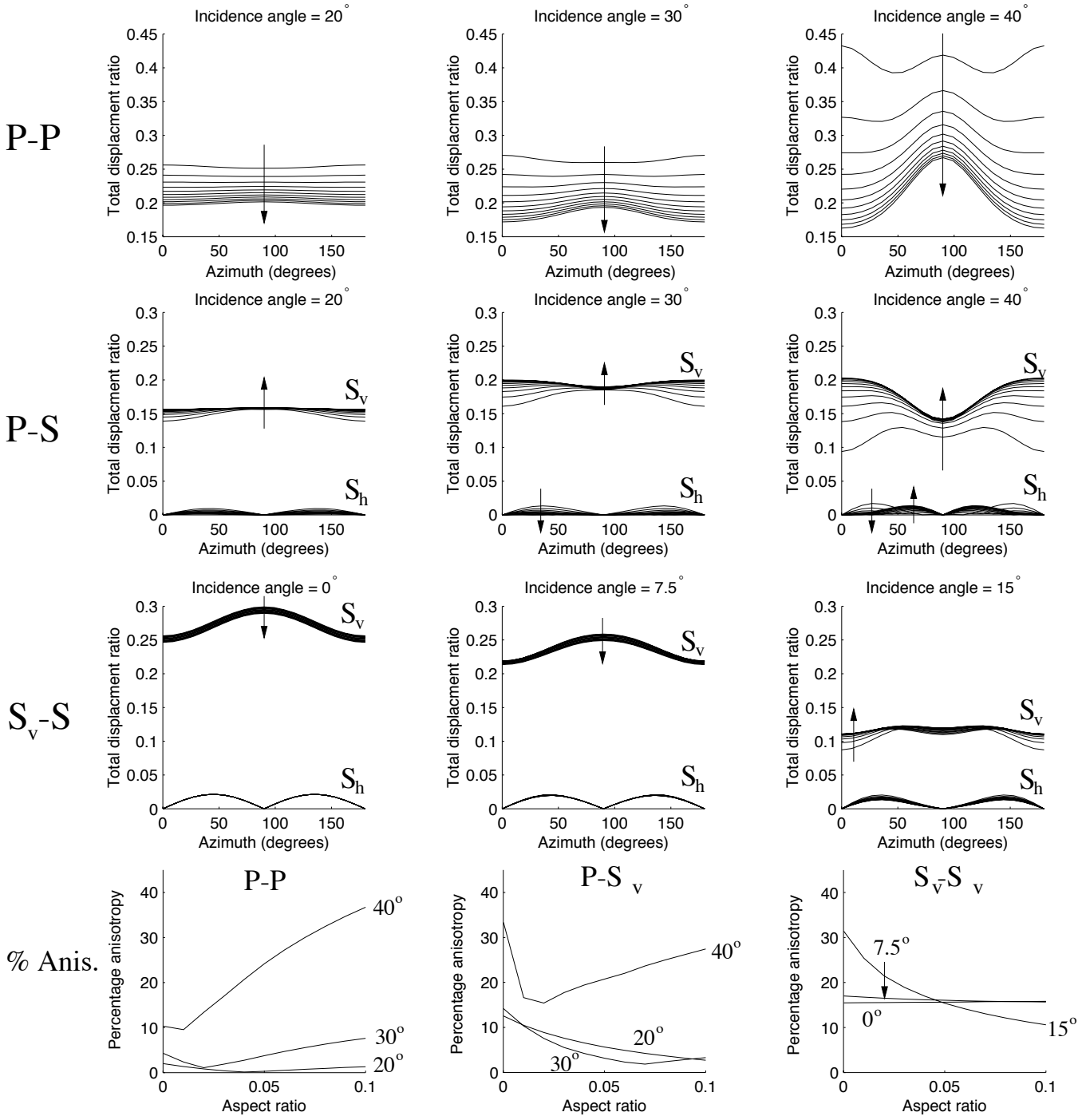

Figure 4: *AVAz curves for P-P and P-S_v reflections with varying aspect ratios and brine-filled fractures. AVAz curves for P-P and P-S_v reflections at* $20^o, 30^o$ *and* 40^o *incidence and for S_v-S_v at* $0^o, 7.5^o$ *and* 15^o *for brine-filled fractures and aspect ratio varying from 0.0001-0.1 in 10 equal steps indicated by the arrows;* $\eta_c = 0.1$. *The three plots at the bottom of the figure indicate the percentage anisotropy observed in each of the AVAz profiles.*

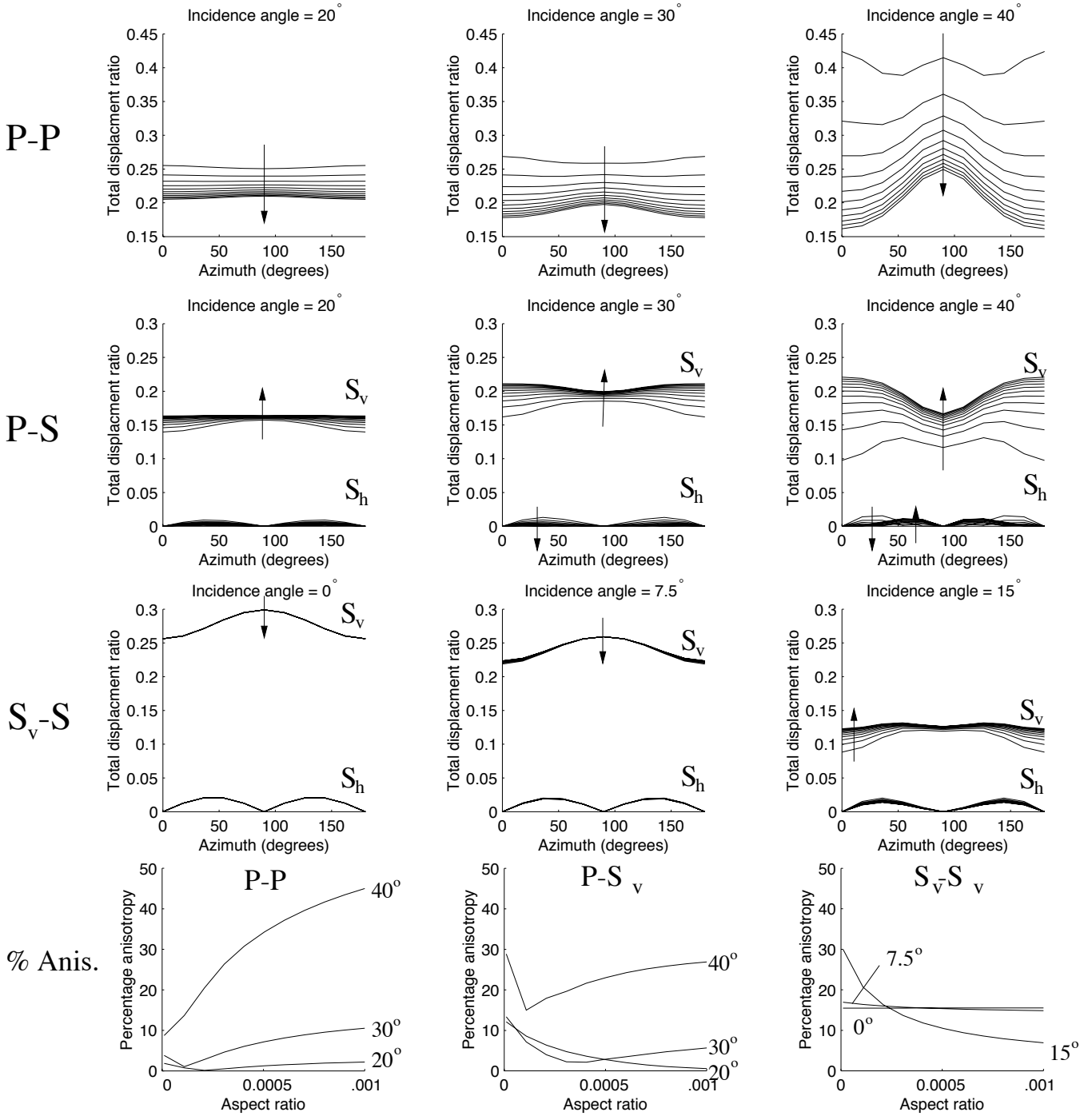

Figure 5: *AVAz curves for P-P and P-S_v reflections with varying aspect ratios and gas-filled fractures. AVAz curves for P-P and P-S_v reflections at $20^o, 30^o$ and 40^o incidence and for S_v-S_v at $0^o, 7.5^o$ and 15^o for gas-filled fractures and aspect ratio varying from 0.00001-0.001 in 10 equal steps indicated by the arrows; $\eta_c = 0.1$. The three plots at the bottom of the figure indicate the percentage anisotropy observed in each of the AVAz profiles.*

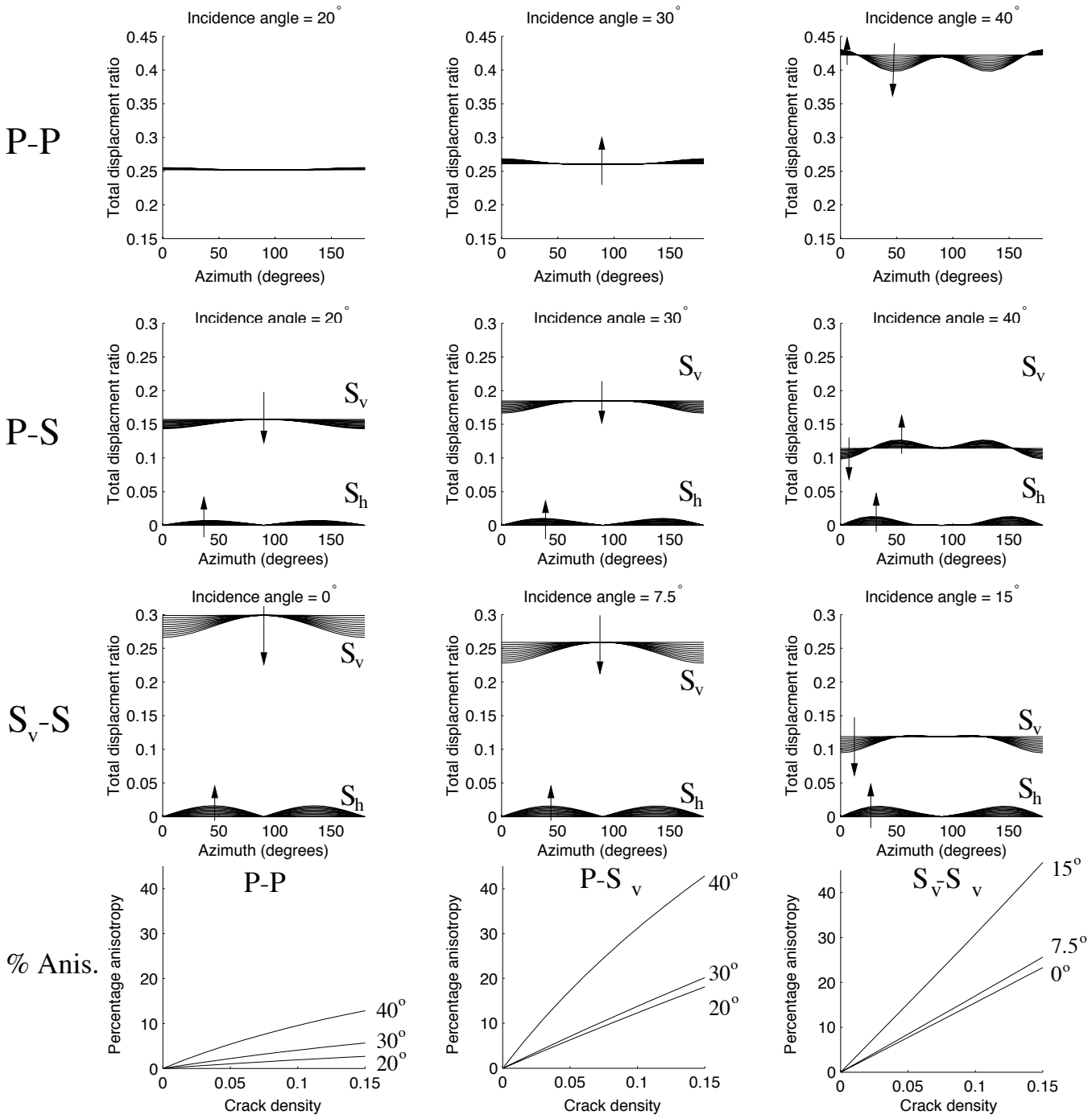

Figure 6: *AVAz curves for P-P and P-S_v reflections with varying crack densities and brine-filled fractures. AVAz curves for P-P and P-S_v reflections at $20^o, 30^o$ and 40^o incidence and for S_v-S_v at $0^o, 7.5^o$ and 15^o for brine-filled fractures and crack density varying from 0.001-0.15 in 10 equal steps indicated by the arrows; d=0.001. The three plots at the bottom of the figure indicate the percentage anisotropy observed in each of the AVAz profiles.*

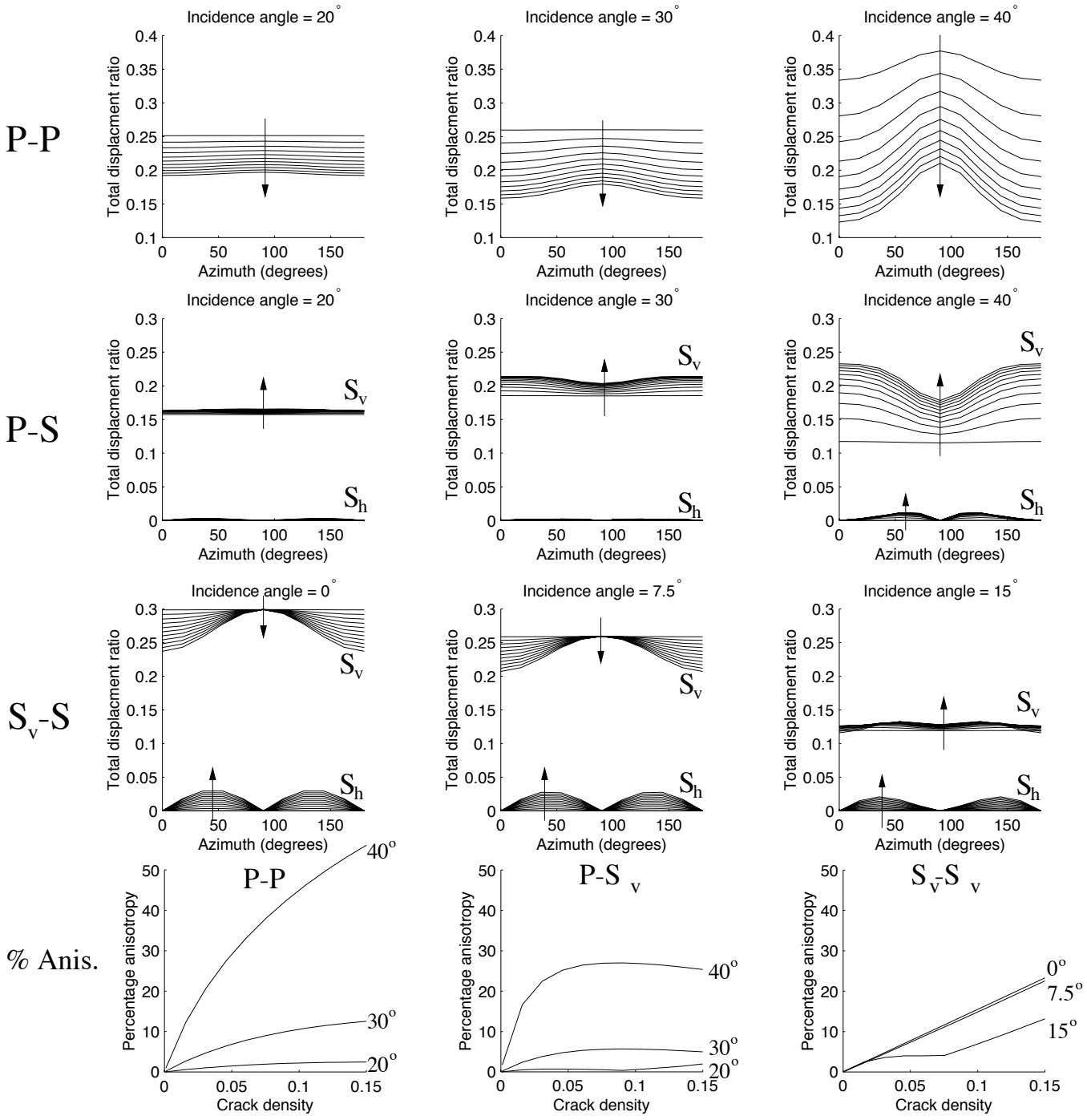

Figure 7: *AVAz curves for P-P and P-S_v reflections with varying crack densities and gas-filled fractures. AVAz curves for P-P and P-S_v reflections at $20^o, 30^o$ and 40^o incidence and for S_v-S_v at $0^o, 7.5^o$ and 15^o for gas-filled fractures and crack density varying from 0.001-0.15 in 10 equal steps indicated by the arrows; d=0.001. The three plots at the bottom of the figure indicate the percentage anisotropy observed in each of the AVAz profiles.*

the aggregate velocity when the crack density, and therefore volume fraction, of gas-filled fractures are changed.

4 AVOA in fractured media with equant porosity

As outlined in the introduction, the presence of hydraulic connectivity between fractures and equant porosity will alter the response of fractures to an applied stress (e.g., Thomsen, 1995). Thus the azimuthal variation of AVO in fractured media with a permeable matrix will be different from that with a non-permeable matrix. The AVAz analysis is therefore extended to include equant porosity using the EFFECT approach to model the effective elasticity (Appendix B).

Figures 8 and 9 show equivalent AVO plots to Figures 2 and 3 but with 1% equant porosity included in the model. The first observation is that the long-offset azimuthal variations are greater, for both the gas and brine filled cases, for the P-P and P-S_v reflections but the S_v-S_v phase appears largely insensitive to the presence of the equant porosity.

Figures 10-11 show how the AVAz changes as the fracture aspect ratio and crack density are varied with equant porosity present. From Figure 10 it can be seen that the variation with aspect ratio is not very sensitive to the introduction of equant porosity, especially for the S_v-S_v phase. However, for the case without equant porosity a rapid increase in anisotropy with increasing aspect ratio was seen, at low aspect ratio, but this does not occur when there is equant porosity.

Figure 11 shows that the crack density becomes a more significant factor when equant porosity is included in the system. Without equant porosity crack density only influenced the magnitude and not the symmetry of the anisotropy. With equant porosity, for P-P reflection and incidence angles greater than about 30^o, there is a negative $\cos 2\phi$ azimuthal variation for low crack density. However with increased crack density there appears to be a significant $\cos 4\phi$ component also. At smaller crack densities there is a negative $\cos 2\phi$ variation. For a 20^o angle of incidence a positive $\cos 2\phi$ trend dominates for larger crack density but the anisotropy is small. The P-S_v phase shows a similar dependence on crack density to the P-P phase. The S_v-S_v phase shows a consistent negative $\cos 2\phi$ variation, for offsets less than 15^o, with little sensitivity to changes in the fracture parameters. Figure 12 shows that increasing the degree of equant porosity produces a very similar result to increasing the aspect ratio (Figure 10).

5 Constraints on interpretation of P-wave AVOA for fracture characterisation

The previous section has shown P-P AVOA data to be highly model dependent and variations with azimuth by a combination of positive- or negative-$\cos 2\phi$ and $\cos 4\phi$ were observed. However, as highlighted in the introduction, many studies are based on the assumption of only a $\cos 2\phi$ azimuthal variation in AVO. The analytical equations, (3) and (4), provide a means for assessing the validity of this approximation and for quantifying some of the observations made in the previous section. Only P-waves are considered here since these are the primary interest in recent studies where P-P AVOA data are analysed and interpreted for fracture characteristics e.g., Hall et al., 2000a;b). Future work should seek to provide equivalent simplified AVOA equations for the P-S and S-S reflections to allow a similar analysis to be applied. Primarily this section seeks to determine when the elliptical AVAz assumption is valid and when the $\cos 2\phi$ variation is positive or negative.

To gain insight into the dependence of the P-wave AVOA on the model parameters equations (3) and (4) may be given in terms of the host rock parameters and fracture variables. Since the major-

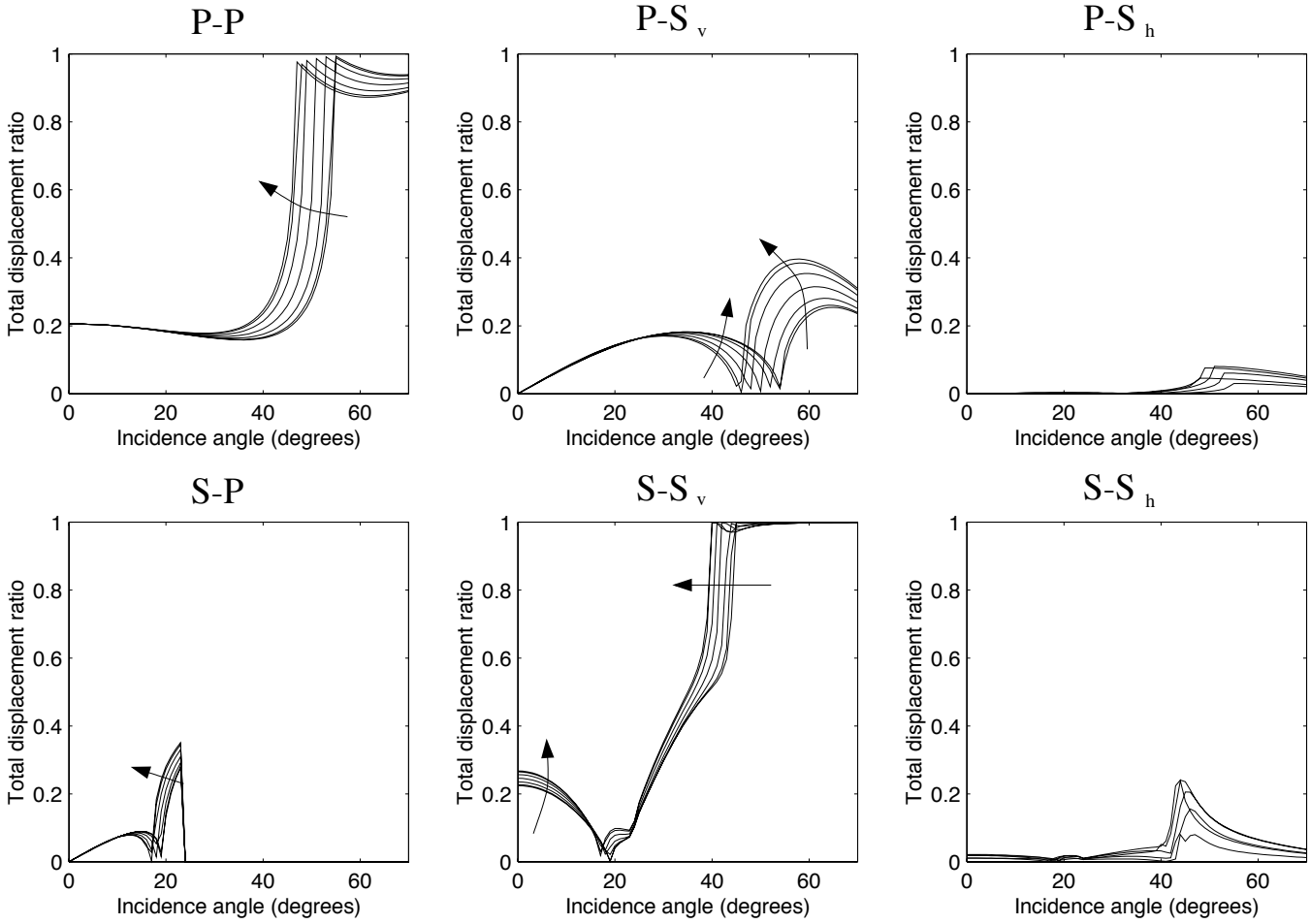

Figure 8: *AVO curves for incident P and S_v at different azimuths relative to a single set of brine-filled fractures in the presence of equant porosity. AVO curves for incident P and S_v and all possible reflection phases at $0^o, 15^o, 30^o, 45^o, 60^o$ and 90^o azimuth relative to the fracture normal direction (arrows indicate increasing azimuth) for aligned brine-filled fractures in the presence of equant porosity; d=0.001 , $\eta_c = 0.1$ and $\phi_p = 0.01$. Note that, as before, S_v and S_h refer to the vertical and horizontal components of a single reflected shear-wave.*

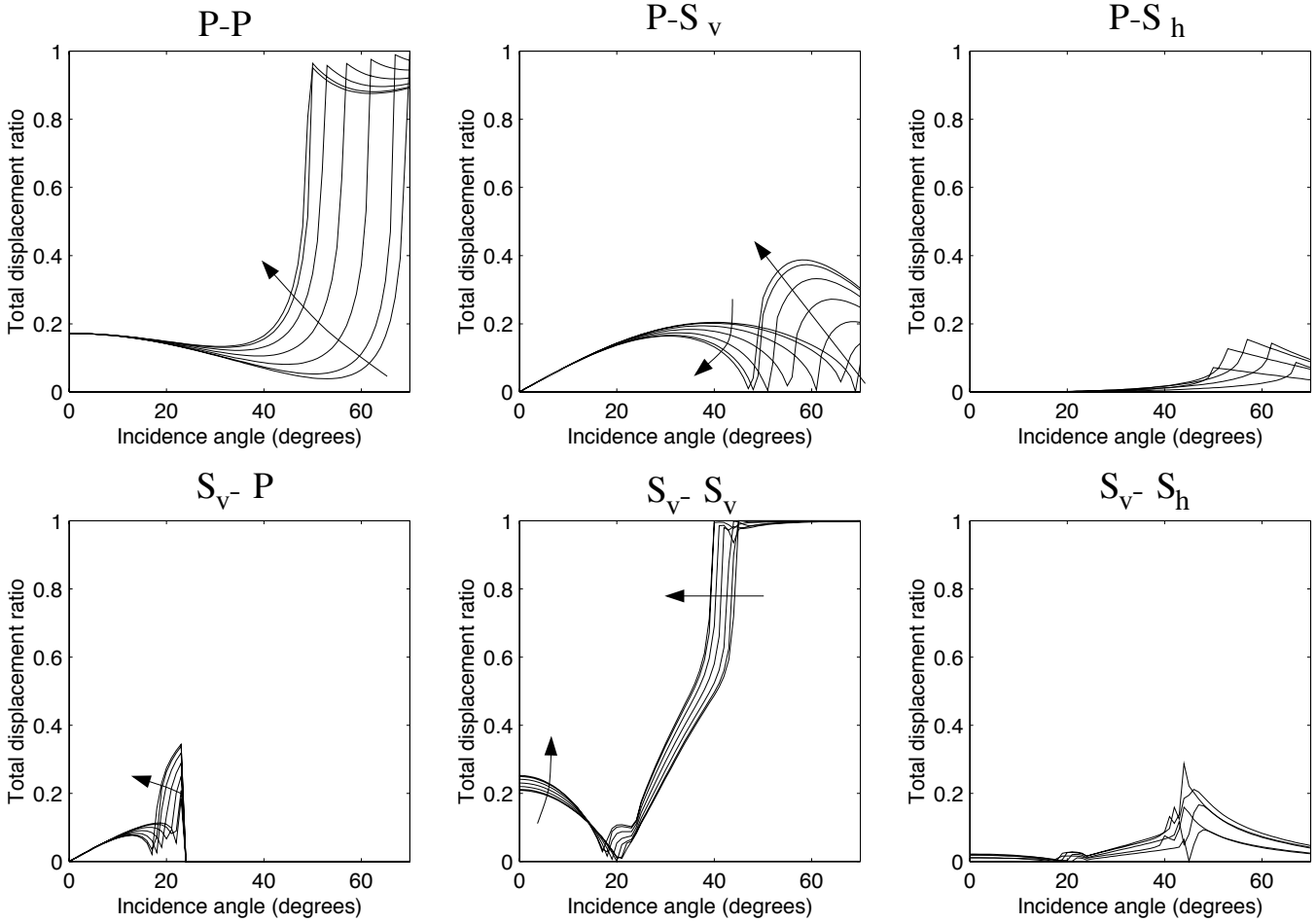

Figure 9: *AVO curves for incident P and S_v at different azimuths relative to a single set of gas-filled fractures in the presence of equant porosity. AVO curves for incident P and S_v and all possible reflection phases at $0^o, 15^o, 30^o, 45^o, 60^o$ and 90^o azimuth relative to the fracture normal direction (arrows indicate increasing azimuth) for aligned gas-filled fractures in the presence of equant porosity; d=0.001, $\eta_c = 0.1$ and $\phi_p = 0.01$. Note that, as before, S_v and S_h refer to the vertical and horizontal components of a single reflected shear-wave.*

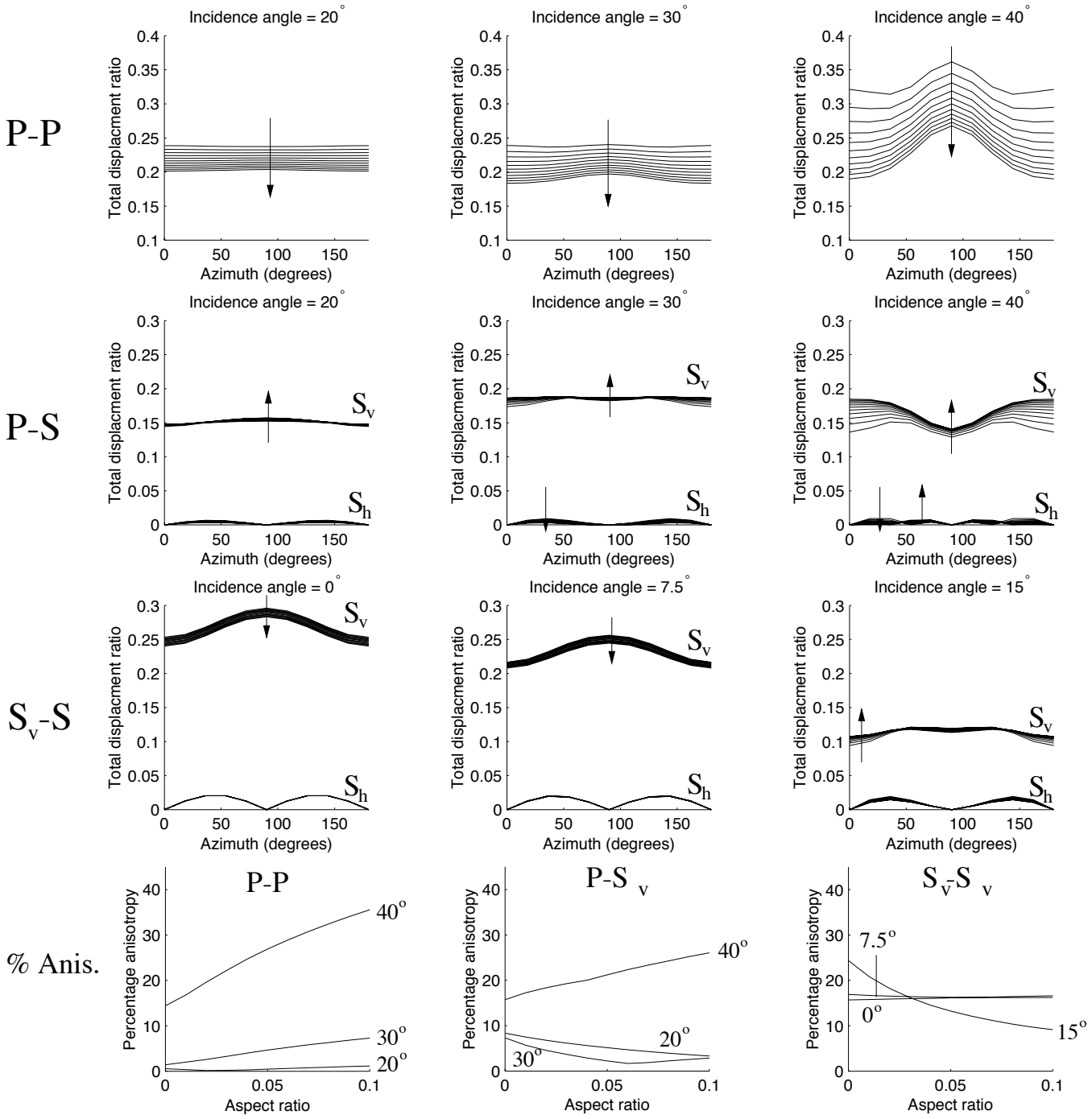

Figure 10: *AVAz curves for P-P and P-S_v for a single set of brine-filled fractures in the presence of equant porosity and varying aspect ratio. AVAz curves for P-P and P-S_v reflections at $20^o, 30^o$ and 40^o incidence and for S_v-S_v at $0^o, 7.5^o$ and 15^o for brine-filled fractures in the presence of equant porosity and aspect ratio varying from 0.0001-0.1 in 10 equal steps indicated by the arrows; $\eta_c = 0.1$, $\phi_p = 0.01$. The three plots at the bottom of the figure indicate the percentage anisotropy observed in each of the AVAz profiles.*

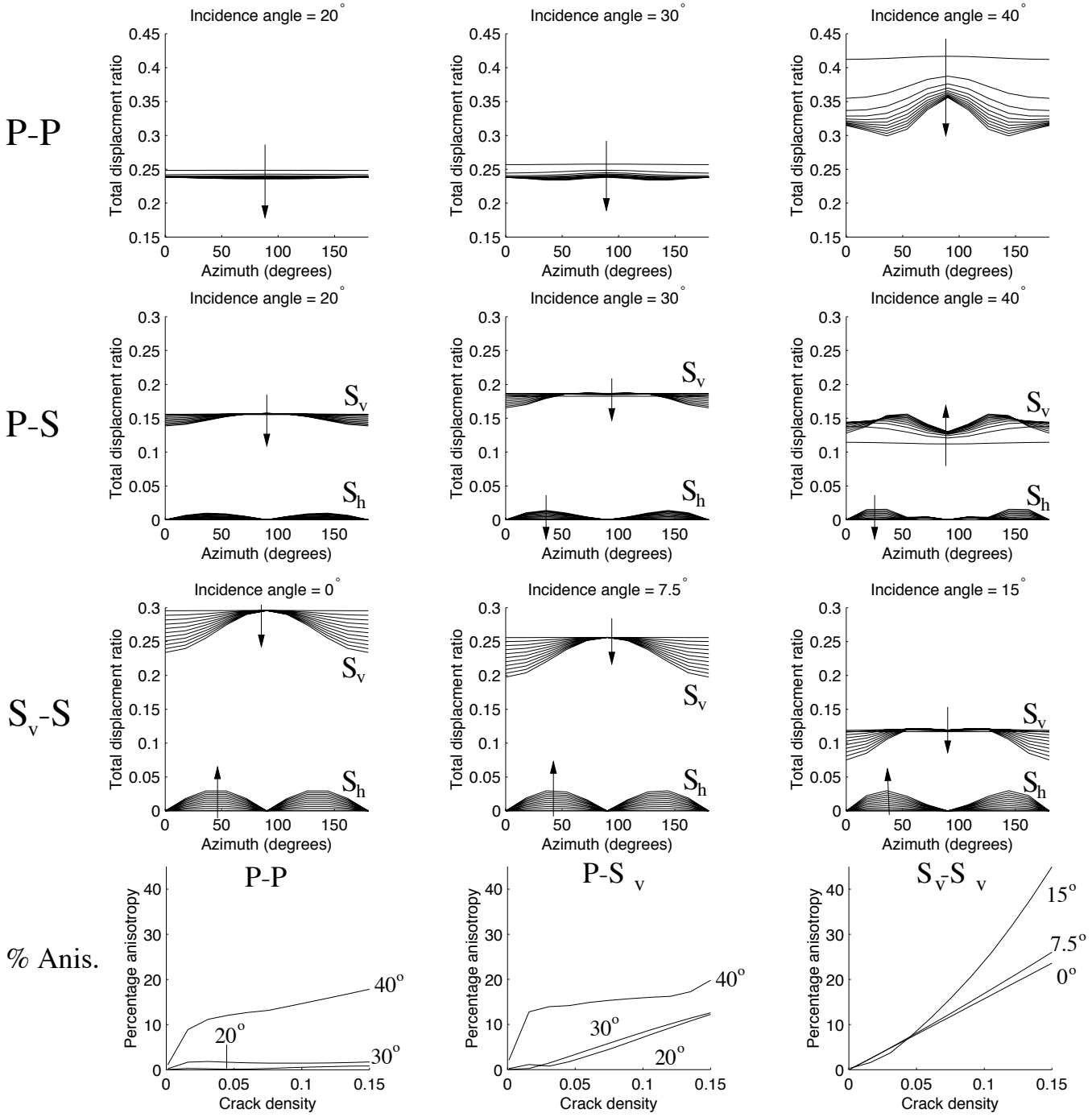

Figure 11: *AVAz curves for P-P and P-S_v for a single set of brine-filled fractures in the presence of equant porosity and varying crack density. AVAz curves for P-P and P-S_v reflections at $20^o, 30^o$ and 40^o incidence and for S_v-S_v at $0^o, 7.5^o$ and 15^o for brine-filled fractures in the presence of equant porosity and crack density varying from 0.001-0.15 in 10 equal steps indicated by the arrows; d=0.001, $\phi_p = 0.01$. The three plots at the bottom of the figure indicate the percentage anisotropy observed in each of the AVAz profiles.*

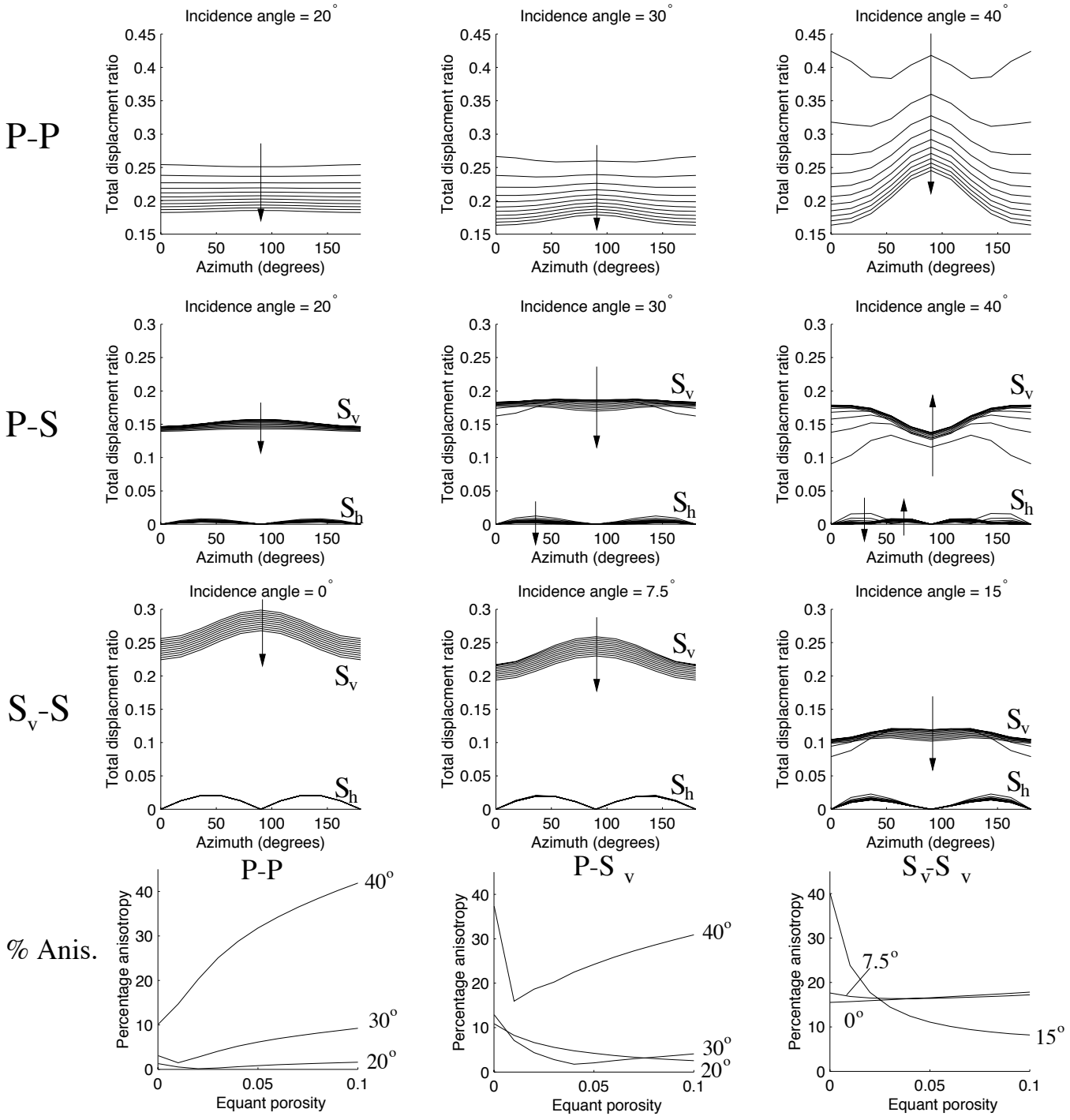

Figure 12: *AVAz curves for P-P and P-S_v for a single set of brine-filled fractures with varying degrees of equant porosity. AVAz curves for P-P and P-S_v reflections at* $20^o, 30^o$ *and* 40^o *incidence and for S_v-S_v at* $0^o, 7.5^o$ *and* 15^o *for brine-filled fractures in the presence of equant porosity varying from 0.0001-0.1 in 10 equal steps indicated by the arrows; d=0.001,* $\eta_c = 0.1$. *The three plots at the bottom of the figure indicate the percentage anisotropy observed in each of the AVAz profiles.*

ity of the information that may be gained about fracturing is determined from the azimuthal variation in the AVO only the coefficients of the azimuthally varying terms are considered in this discussion. This is achieved using the Thomsen parameters given in Appendix A (equations A.1-A.3) with a further weak anisotropy assumption that $\epsilon^{(v)} \approx -\epsilon^r$ and $\delta^{(v)} \approx (\delta^r - 2\epsilon^r)$ (Rüger, 1998). Therefore, for an isotropic medium over a vertically fractured medium, the coefficient of $\cos 2\phi$, from equation (3), is given as

$$\frac{1}{2}\left[\delta^r - 2\epsilon^r + 2\left(\frac{2\overline{\beta}}{\overline{\alpha}}\right)^2 \gamma - \epsilon^r \tan^2 i\right] \sin^2 i, \quad (6)$$

and the coefficient of $\cos 4\phi$ is

$$\frac{1}{8}(3\epsilon^r - 2\delta^r) \tan^2 i \sin^2 i. \quad (7)$$

Using equations (B.14) and (B.15), these coefficients are written in terms of the additional fracture compliances of Schoenberg and Sayers (1005), Z_N and Z_T, (see Appendix B) for the coefficient of $\cos 2\phi$,

$$\frac{1}{2}\left[-Z_N M_b \left(\frac{2\nu_b + \tan^2 i}{2(1-\nu_b)^2}\right) + Z_T \mu_b \left\{4\left(\frac{\overline{\beta}}{\overline{\alpha}}\right)^2 - \left(\frac{1-2\nu_b}{1-\nu_b}\right)\right\}\right] \sin^2 i, \quad (8)$$

and the coefficient of $\cos 4\phi$,

$$\frac{1}{8}\left(\frac{1-2\nu_b}{1-\nu_b}\right)\left[Z_N M_b \left(\frac{1+2\nu_b}{2(1-\nu_b)}\right) - Z_T \mu_b\right] \tan^2 i \sin^2 i. \quad (9)$$

In these equations, $M_b = (\lambda_b + 2\mu_b)$ where λ_b and μ_b are the lamé parameters and ν_b the Poissons ratio of the isotropic background medium of the fractured unit.

Equations (8) and (9) indicate that if the background P- and S-wave velocities of the unfractured material bounding the reflecting interface are known, the only factors which affect the nature of the azimuthal variation in AVO are the normal and tangential fracture compliances of the fractured medium. This result could be useful in the inversion of AVOA data if the AVAz signature can be separated into the $\cos 2\phi$ and $\cos 4\phi$ components as in equations (8) and (9). This may be possible through Fourier analysis of the AVAz for a fixed offset as demonstrated by Sayers (1999) for noise-free synthetic data.

It has been highlighted in the preceding discussion that there could be an ambiguity in the determination of fracture orientation due to the changing sign of the near-offset AVAz trend. For example, from equation (8), increasing the incidence angle or fracture-normal compliance will lead to a more negative $\cos 2\phi$ term since the negative part of the coefficient will be increased. Additionally it has been suggested previously (e.g., Mallick et al., 1998) that the variation in AVOA will be elliptical but it has been shown in this work that there could be a significant $\cos 4\phi$ component to the AVOA in some situations. To investigate the changing sign of the $\cos 2\phi$ term and also when a $\cos 4\phi$ trend must be considered the magnitudes of the coefficients from equations (8) and (9) are plotted for a range of crack densities, aspect ratios and equant porosity values in Figures 13 and 14.

Figures 13 and 14 show that, in general, when there is no equant porosity, both the $\cos 2\phi$ and $\cos 4\phi$ terms have an approximately linear scaling with respect to the crack density. Furthermore, an increasingly negative $\cos 2\phi$ term is seen as the aspect ratio is increased (corresponding to an increasing fracture-normal compliance) so that a change from positive to negative $\cos 2\phi$ occurs and in this region the $\cos 4\phi$ term will dominate. With gas-filled fractures the switch to a negative $\cos 2\phi$ variation occurs at an aspect ratio of about 0.0005 which is much lower than for the brine-filled case where the switch occurs for aspect ratios between about 0.02 and 0.03. Furthermore there is a greatly reduced sensitivity to aspect ratio for values greater than about 0.001 when there is a gas fill.

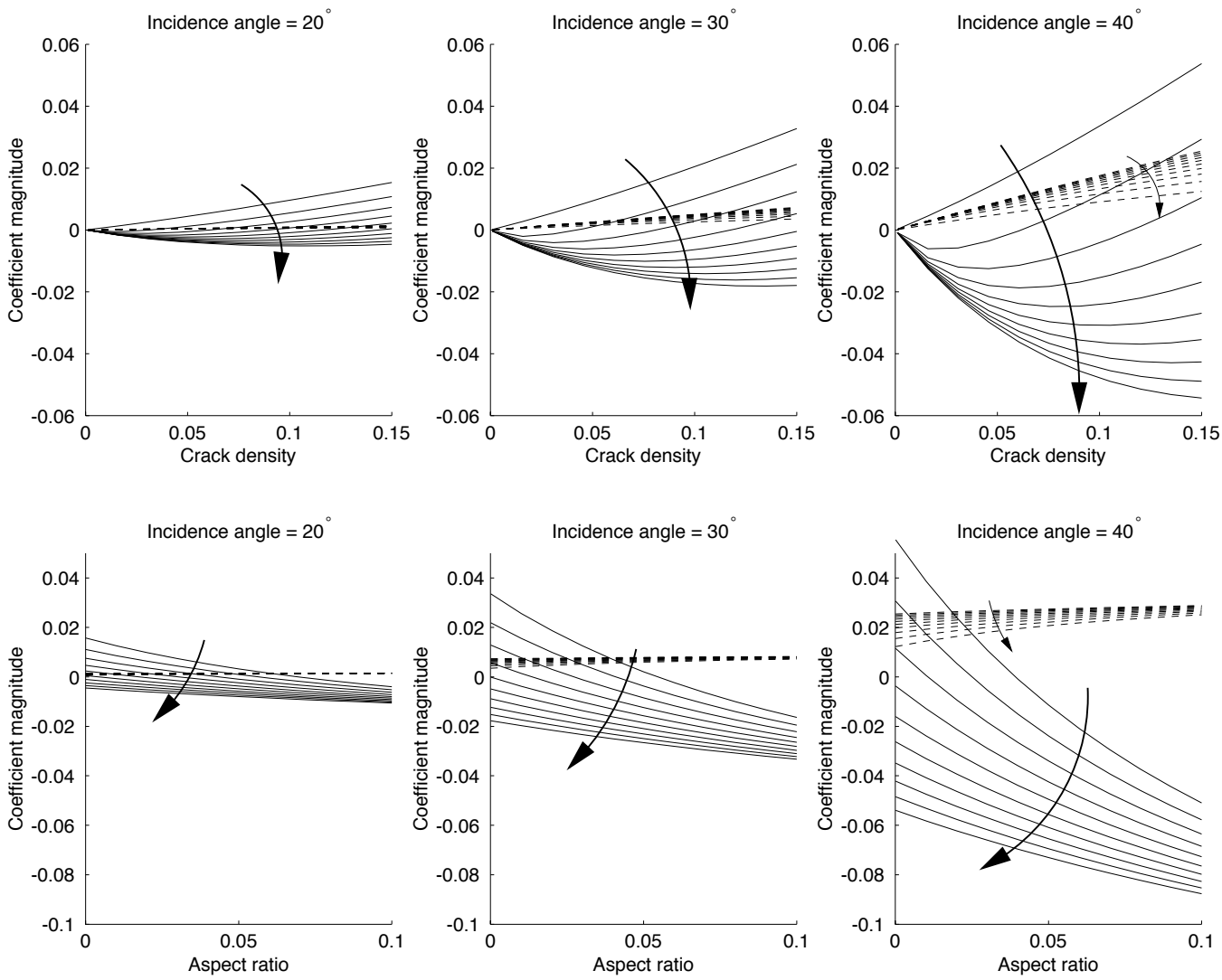

Figure 13: *Comparison of the magnitudes of the* $\cos 2\phi$ *and* $\cos 4\phi$ *components of the P-wave AVAz for brine-filled fractures with varying crack density and aspect ratio and different degrees of equant porosity. Comparison of the magnitudes of the* $\cos 2\phi$ *(solid lines) and* $\cos 4\phi$ *(dashed lines) components of the P-wave AVAz for reflections at the top of a fractured permeable chalk with brine-filled fractures and varying crack density or aspect ratio at incidence angles of* $20^o, 30^o$ *and* 40^o *and different degree s of equant porosity (*ϕ_p *varies from 0.0-0.1 in 10 equal steps as indicated by the arrows).*

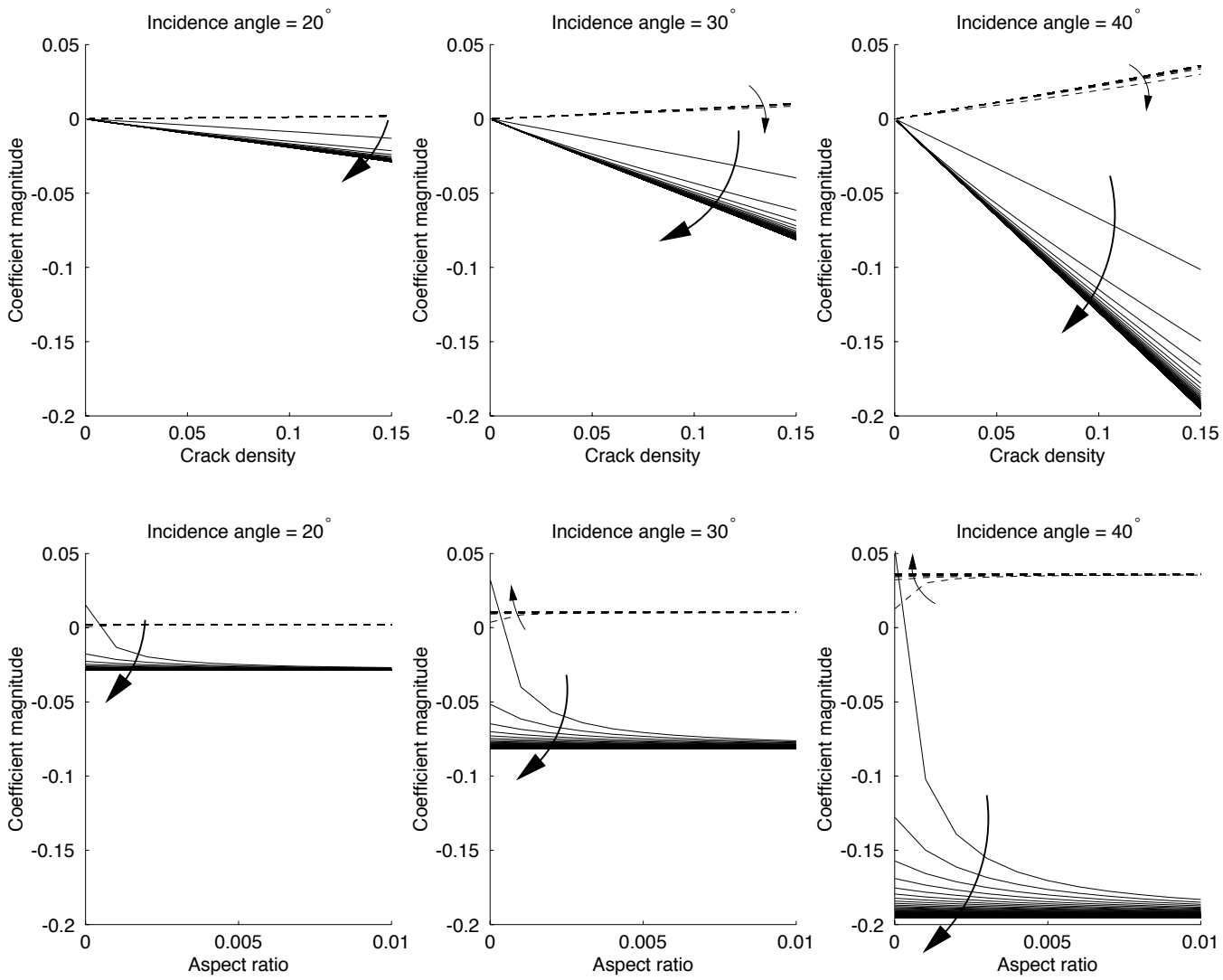

Figure 14: *Comparison of the magnitudes of the* $\cos 2\phi$ *and* $\cos 4\phi$ *components of the P-wave AVAz for gas-filled fractures with varying crack density and aspect ratio and different degrees of equant porosity. Comparison of the magnitudes of the* $\cos 2\phi$ *(solid lines) and* $\cos 4\phi$ *(dashed lines) components of the P-wave AVAz for reflections at the top of a fractured permeable chalk with gas-filled fractures and varying crack density or aspect ratio at incidence angles of* $20^o, 30^o$ *and* 40^o *and different degrees of equant porosity (*ϕ_p *varies from 0.0-0.1 in 100 equal steps as indicated by the arrows).*

With equant porosity it is seen that the sensitivity to aspect ratio is reduced as the degree of equant porosity is increased. However, crack density becomes a more important term, especially for brine-filled fractures. As the amount of equant porosity is increased further the sensitivity to crack density is, however, also reduced.

This section has shown that the azimuthal variation in P-P AVO is often dominated by a $\cos 2\phi$ variation with azimuth, especially for gas-filled fractures and at near offsets, but this trend could be positive or negative. The assumption of an elliptical P-P AVAz variation may therefore often provide a fracture orientation direction but the actual direction of the fracture strike, as opposed to the perpendicular direction, will be ambiguous. However it is possible that this characteristic could be utilised to detect changes in the fluid-fill of the fractures (e.g., MacBeth, 2000).

If longer offsets are used in the analysis the AVAz may possess a significant $\cos 4\phi$ variation (only for a small subset of models, i.e., brine-filled fractures with aspect ratios around 0.02-0.03 and low equant porosity will there be a $\cos 4\phi$ dependence at near-offsets; see Figures 13 and 14). Thus approaches based on an elliptical AVAz assumption may not always determine a clear fracture orientation and the result could depend largely on which azimuths are sampled. Furthermore, this section has highlighted that P-P AVOA contains significant information on fracture properties, particularly at these long offsets, which may provide greater insight than would be obtained from any near-offset data or shear-waves. Therefore it would be desirable in the future to utilise these longer offsets but this will require well constrained rock property models due to the model dependent nature of these variations.

6 AVOA in the presence of multiple-fracture alignment

Multiple fracture sets could significantly affect the interpretation of AVOA for fracture characteristics or permeability and there is a potential problem as to whether the direction of maximum permeability can be correctly determined using AVOA. Sayers (1998; 1999) briefly considered this problem and suggested that with multiple fracture alignments there may be higher order azimuthal variations in AVO than the previously suggested $\cos 2\phi$ and $\cos 4\phi$ trends (i.e, a $\cos 6\phi$ component may exist also). This section aims to provide insight into AVOA signatures over multiple fracture sets using numerical modelling as presented in the previous sections for a single fracture alignment.

Figures 15 and 16 show the change in AVAz when there is an increase in the inter-fracture angle between two identical, vertical fracture sets which have a brine or gas fill respectively. In general it appears that two sets of identical fractures produce an AVOA signature which is similar to that which would be observed from a single set. The orientation of this "apparent fracture set" is in the direction which bisects the acute inter-fracture angle; this will be referred to as the median azimuth. However at long offsets and with a large inter-fracture angle the P-P and P-S AVOA are different to that from a single fracture alignment. Therefore it may be possible to detect the presence of two discrete, but identical, fracture sets using P-P or P-S AVOA. For liquid-filled fractures this requires an inter-fracture angle greater than about 40^o and for a gas-fill greater than about 70^o. For example, two identical, vertical fracture sets aligned orthogonally to each other produces AVAz with a four-fold rotational symmetry with the higher P-P amplitudes along the fracture parallel directions.

Figures 17-21 show the AVAz profiles for a model where there are two sets of aligned, vertical fractures at 60^o and 120^o azimuth (analogous to a con-

jugate set of fractures). It can be seen from Figure 17 that if the crack density of the two fracture sets is varied by the same amount and all other factors are fixed only the magnitude, and not the symmetry, of the azimuthal variation changes. However, if the aspect ratio of the two fracture sets is changed (Figure 18), and all the other parameters are constant, the AVAZ changes character. For low aspect ratio fractures (less than about 0.03) and angles of incidence around 40^o it is possible to distinguish the P-P and P-S_v AVAz signatures of a conjugate set of fractures from the AVAz due to a single set. For larger aspect ratios the AVAz resembles that due to a single set of fractures aligned along the median azimuth. However, for short-offsets, especially with the S_v-S_v data, the AVAz is similar to that from a single fracture alignment along the median azimuth, for all aspect ratios.

A more likely scenario, involving multiple fracture alignment, is one where the fracture sets are not identical. For example, if there is more than one direction of fracture alignment, one set will often be more open than the others due to the present day stress regime (i.e., fractures parallel to the maximum stress direction will be more open than those perpendicular to it). Therefore one set is likely to have a higher aspect ratio or crack density than the others. Figures 19 and 20 show how the AVAz for brine-filled and dry fractures varies for two sets aligned as above but with the crack density of one set varying. From these figures it is seen that, particularly with the S_v-S_v data, the AVAz resembles that due to a single fracture alignment for all values of crack density but the apparent alignment varies. As the crack density of one set is reduced this apparent alignment moves closer to the azimuth of the fracture set with higher crack density.

Figure 21 shows the case where the aspect ratio of one set is varied whilst all other parameters are constant. It can be seen here that if the aspect ratio of one set is increased the AVAz becomes more like that due to a single fracture alignment centred on an azimuth approaching that of the wider fracture set.

7 Conclusion

The variations in AVOA in fractured media have been investigated through numerical modelling and analytical equations. Single and multiple fracture alignments have been considered for models with an impermeable matrix and models where fractures are hydraulically connected to the surrounding matrix porosity. These examples have indicated that seismic reflectivity can be highly sensitive to the properties (e.g., orientation and density) of aligned fracturing. An advantage of reflectivity methods is that the observed azimuthal variations have a much greater dependence on properties local to a single reflector. Travel-time methods are influenced by the properties along the whole ray-path so the observed anisotropy in travel-time data will be an aggregate effect from all the overlying layers. There must also be a sufficient thickness through which the wave must propagate before substantial variations can be observed in travel-times.

From the detailed observations made in this paper, AVOA appears to be highly model dependent. However, a number of general observations can be made on the sensitivity of AVOA to variations in the fracture parameters; these are summarised below.

Azimuthal variations in AVO in fractured media

Numerical modelling showed that azimuthal variations in AVO have a significant sensitivity to fracture properties. Analytical expressions were presented which allowed quantification of this sensitivity. To aid future interpretation of such data for fracture characteristics some general constraints are highlighted below.

- For fractures with low normal compliance, Z_N, (e.g., fractures with low aspect ratios, a brine fill or high crack density with low matrix porosity) there is more likely to be a $\cos 4\phi$ azimuthal variation in P-P and P-S_v AVOA or, for very low aspect ratio and little equant porosity, a positive $\cos 2\phi$ trend.

- For fractures which have a large Z_N compliance (e.g., those with higher aspect ratio, a gas fill or in the presence of high equant porosity) the P-P and P-S_v AVAZ are more likely to show a negative $\cos 2\phi$ trend.

- In general, when there is no equant porosity it is seen that aspect ratio is the most important factor in defining the azimuthal symmetry in AVOA. In this case, crack density has no influence on the symmetry of the azimuthal variations and only changes the magnitude.

- When equant porosity is included in the system the fractures are more compliant and crack density becomes the most significant factor in defining the azimuthal symmetry in AVOA. However, this effect is less pronounced with dry fractures which are already highly compliant.

- S_v-S AVOA shows little sensitivity to changes in rock and fracture parameters but provides significant, consistent indications of fracture orientation at near offsets.

AVOA in media with multiple fracture alignments

Modelling in this work also considered the case where there are two different alignments of fractures. This showed that P-P and P-S_v AVOA are the attributes that are most sensitive to the inter-fracture angles and fracture properties when there is more than one set of fractures. If there are two identical sets of parallel fractures they will be distinguishable, using azimuthal trends in AVOA, from a single fracture alignment for low compliance fractures (e.g., fractures with low aspect ratio) and a large inter-fracture angle. If there are two sets of fractures which are not identical the AVOA signatures will resemble that from a single fracture set with an alignment nearer the azimuth of the fracture set with higher crack density or larger aspect ratio. These observations indicate that AVOA will in general provide an accurate prediction of the direction of maximum permeability.

P-P vs P-S vs S-S AVOA for fracture characterisation

One of the aims of this work was to determine if P-waves alone could be used to characterise aligned fracturing. P-P and P-S_v AVOA have been shown to have the most potential for fracture characterisation. Due to the complicated nature of these phases (i.e., the trade-off between $\cos 2\phi$ and $\cos 4\phi$ terms which is sensitive to the fracture characteristics) there is potentially more information to be gained from these data than from, say, shear-wave splitting analysis. It is also observed that the P-P AVOA shows greater anisotropy and sensitivity to changing crack density for gas-filled fractures whilst P-S_v AVOA appears to better for liquid-filled fractures. The shear-wave (S_v-S) AVOA shows critical reflections at much shorter offsets than with incident P-waves but significant azimuthal variations are observed in these data which will provide strong indications of fracture orientation but little insight into other fracture properties.

References

Aki, K. and Richards, P.G., 1980, Quantitative seismology: theory and methods: W. H. Freeman.

Budiansky, B. and O'Connell, R.J., 1980, Bulk dissipation in heterogeneous media: Solid earth geophys. and geotech., 42, 1–10.

Castagna, J.P. and Backus, M., 1993, Offset-dependent reflectivity - Theory and practice of AVO analysis: Soc. Expl. Geophys.

Castagna, J.P. and Swan, H.W., 1997, Principles of AVO crossplotting: Leading Edge, 16(04), 337–342.

Chapman, C.H., 1976, Exact and approximate gen-

eralized ray theory in vertically inhomogeneous media: Geophys. J. Roy. Astr. Soc., 46, 201–233.

Crampin, S., 1984, Effective anisotropic elastic constants for wave propagation through cracked solids: Geophys. J. Roy. Astr. Soc., 76, 135–145.

Crampin, S. and Lovell, J.H., 1991, A decade of shear-wave splitting in the earth's crust: what does it mean? what use can we make of it? and what should we do next? Geophys. J. Int., 107, 387–407.

Crampin, S., McGonigle, R., and Ando, M., 1986, Extensive-dilatancy anisotropy beneath Mount Hood, Oregon and the effect of aspect ratio on seismic velocities through aligned cracks. J. Geophys. Res., 91, 12703–12710.

Guest, W. S., 1993, Reflection, transmission and conversion of elastic waves in inhomogeneous anisotropic media: Theory and application to crustal seismic surveys: PhD thesis, Queen's University, Ontario, Canada.

Guest, W. S. and Kendall, J-M., 1993, Modelling seismic waveforms in anisotropic inhomogeneous media using ray and maslov asymptotic theory: Applications to exploration seismology: In Lawton, D. C., editor, 5th Int. Worksh. on Seismic Anisotropy, Volume 29, pages 78–92. J. Can. Soc. Expl. Geophys.

Guest, W. S., Spencer, C., and Thomson, C.J., 1993, Anisotropic reflection and transmission calculations with application to a crustal seismic survey from the East Greenland Shelf: J. Geophys. Res., 98, 14161–14184.

Hall, S.A., 2000, Rock fracture characterisation and seismic anisotropy: application to ocean bottom sesmic data: PhD thesis, University of Leeds, Leeds, England.

Hall, S.A., Barkved, O.I., Mueller, M.C., and Kendall, J-M., 2000a, An approach for P-wave AVOA in 3D-OBC data: In 62nd Mtg. Eur. Assoc. Expl Geophys., Expanded Abstracts, pages Paper: C–09.

Hall, S.A. and Kendall, J-M., 1999, A methodology for ocean bottom AVOA analysis using common receiver data: In 69th Annual Internat. Mtg., Soc. Expl. Geophys., Expanded Abstracts, pages 856–859.

Hall, S.A., Kendall, J-M., Barkved, O.I., and Mueller, M.C., 2000b, Fracture characterisation using P-wave AVOA in 3D-OBC data: In 70th Annual Internat. Mtg., Soc. Expl. Geophys., Expanded Abstracts.

Harwood, S., Rowbotham, P.S., Bush, I., Williamson, P.R., Houllevigue, H., and Kendall, J-M., 1998, Uncertainties in the analysis of AVOA for determination of fracture orientation: In Proc. 8th Int. Worksh. Seismic Anisotropy, Rev. Inst. Franc. Petr., 53, pages 621–628.

Hoenig, A., 1978, Elastic moduli of a non-randomly cracked body: Int. J. Solids Structures, 15, 137–154.

Horne, S., MacBeth, C., Queen, J., Rizer, W., and Cox, V., 1997, Fracture characterisation from near-offset VSP inversion: Geophys. Prosp., 45, 141–164.

Hudson, J.A., 1980, Overall properties of a cracked solid: Math. Proc. Camb. Phil. Soc., 88, 371–384.

Hudson, J.A., 1981, Wave speeds and attenuation of elastic waves in material containing cracks: Geophys. J. Roy. Astr. Soc., 64, 133–150.

Hudson, J.A., 1986, A higher order approximation to the wave propagation constants for a cracked solid: Geophys. J. Roy. Astr. Soc., 87, 265–274.

Hudson, J.A., Liu, E., and Crampin, S., 1996, Mechanical properties of materials with interconnected cracks and pores: Geophys. J. Int., 124, 105–112.

Kendall, R.R. and Kendall, J-M., 1996, Shear-wave amplitude anomalies in south-central Wyoming: Leading Edge, 15, 913–920.

Li, X-Y., 1997, Viability of azimuthal variation in P-wave moveout for fracture detection: In 67th Annual Internat. Mtg., Soc. Expl. Geophys., Expanded Abstracts, 1555–1558.

Lynn, H. B., Simon, K. M., Bates, C. R., Layman, M., Schneider, R., and Jones, M., 1995, Use of anisotropy in P-wave and S-wave data for fracture characterization in a naturally fractured gas reservoir: Leading Edge, 14, 887–893.

MacBeth, C., 2000, Combining P-P AVOA and NMO distinguishes gas from water in fractures: In Proc. 9th Int. Worksh. Seismic Anisotropy, page 5.

Macbeth, C., Jakubowicz, H., Kirk, W., Li, X-Y., and Ohlsen, F., 1999, Fracture-related amplitude variations with offset and azimuth in marine seismic data: First Break, 17, 13–26.

Mallick, S., Craft, K.L., Meister, L.J., and Chambers, R.E., 1998, Determination of the principal directions of azimuthal anisotropy from P-wave seismic data: Geophysics, 63, 692–706.

Mueller, M.C., 1991, Prediction of lateral variability in fracture intensity using multicomponent shear-wave surface seismic as a precursor to horizontal drilling in the austin chalk: Geophys. J. Int., 107, 409–415.

Ostrander, W.J., 1984, Plane-wave reflection coefficients for gas sands at non-normal angles of incidence: Geophysics, 49, 1637–1648.

Potters, J.H.H.M., Groenendaal, H.J.J., Oates, S.J., Hake, J.H., and Kalden, A.B., 1999, The 3D shear experiment over the Natih filed in Oman. Reservoir geology, data acquisition ans anisotropy analysis. Geophys. Prosp., 47, 637–662.

Rüger, A., 1998, Variation of P-wave reflectivity with offset and azimuth in anisotropic media: Geophysics, 63, 935–947.

Rutherford, S. and Williams, R., 1989, Amplitude-versus-offset variations in gas sands: Geophysics, 54, 680–688.

Sayers, C.M., 1998, Misalignment of the orientation of fractures and the principal axes for P and S waves in rocks containing non-orthogonal fracture sets: Geophys. J. Int., 133, 459–466.

Sayers, C.M., 1999, Azimuth-dependent AVO in reservoirs containing non-orthogonal fracture sets: In Abstracts of "Fracture characterization and imaging" post-convention workshop, 69th Ann. Internat. Mtg., Soc. Expl. Geophys.

Schoenberg, M. and Sayers, C.M., 1995, Seismic anisotropy of fractured rock: Geophysics, 60, 204–211.

Shuey, R.T., 1985, A simplification of the Zoeppritz equations: Geophysics, 60, 609–614.

Thomsen, L., 1986, Weak elastic anisotropy: Geophysics, 51, 1954–1966.

Thomsen, L., 1988, Reflection seismology over azimuthally anisotropic media: Geophysics, 53, 304–313.

Thomsen, L., 1993, Weak anisotropic reflections, in 'Offset-dependent reflectivity - Theory and practice of AVO analysis,' Castagna, J.P. and Backus, M., [Eds].: Soc. Expl. Geophys.

Thomsen, L., 1995, Elastic anisotropy due to aligned cracks in porous rock: Geophys. Prosp., 43, 805–829.

Vavryčuk, V. and Pšenčík, I., 1998, PP-wave reflection coefficients in weakly anisotropic elastic media: Geophysics, 63, 2129–2141.

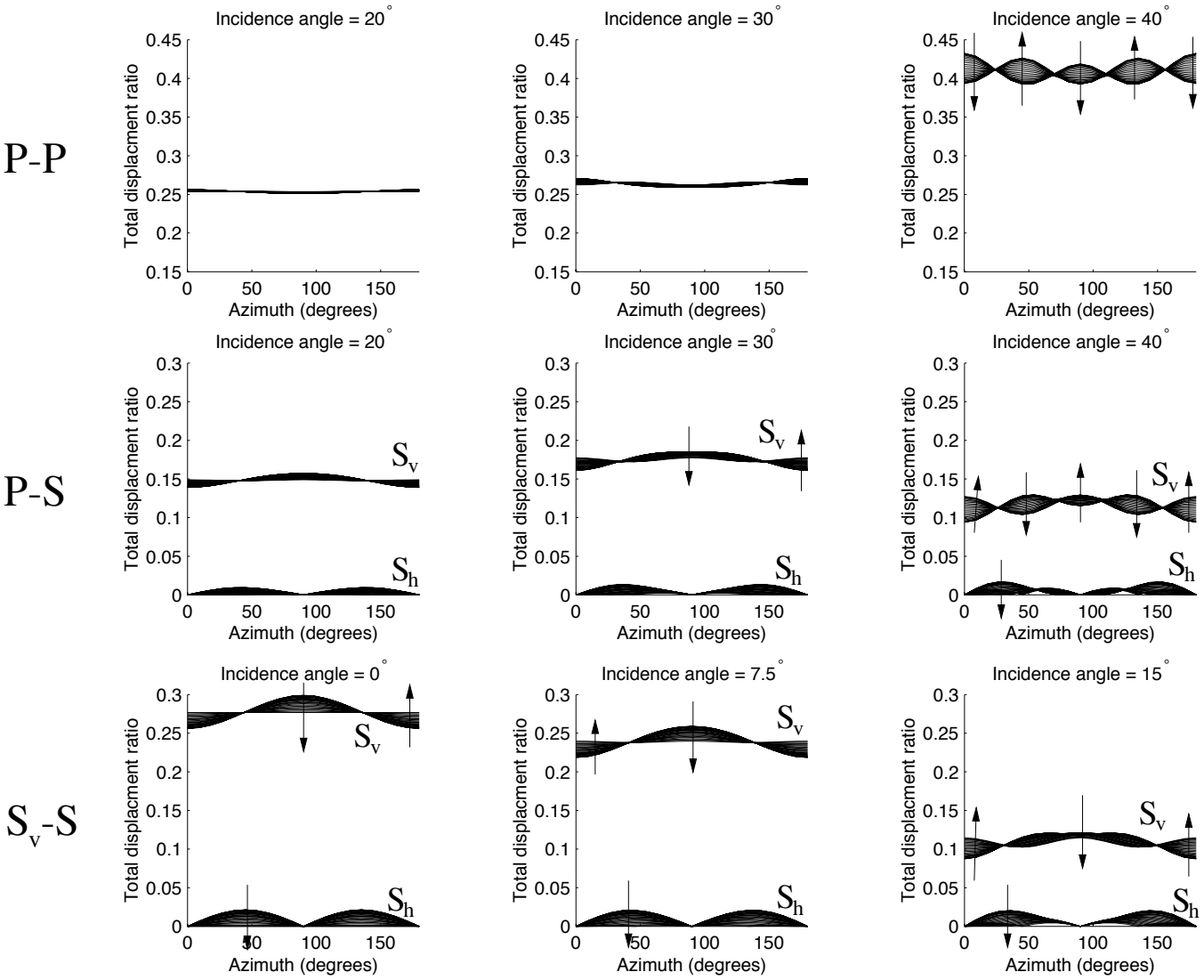

Figure 15: *P-P and P-S_v AVAz for two sets of identical, vertical, brine-filled fractures with different alignments and varying inter-fracture angle. AVAz curves for P-P and P-S_v reflections at $20^o, 30^o$ and 40^o incidence and for S_v-S_v at $0^o, 7.5^o$ and 15^o for two sets of identical, vertical, brine-filled fractures with different alignments and the inter-fracture angle varying from $0 - 90^o$ (with the angle-bisector along 90^o azimuth) in 10 equal steps, as indicated by the arrows; d=0.001, $\eta_c = 0.05$ for each set.*

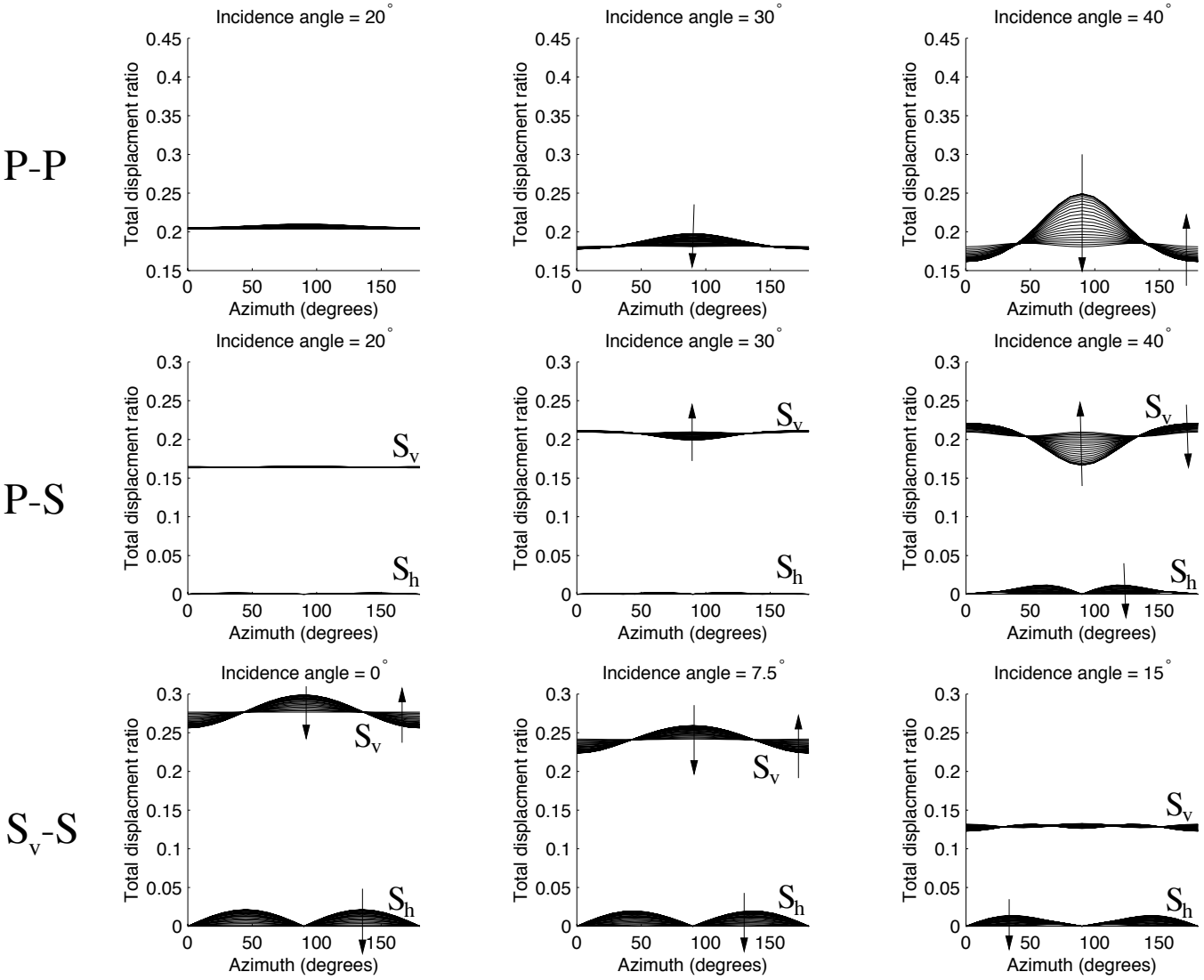

Figure 16: *P-P and P-S_v AVAz for two sets of identical, vertical, gas-filled fractures with different alignments and varying inter-fracture angle. AVAz curves for P-P and P-S_v reflections at* $20^o, 30^o$ *and* 40^o *incidence and for S_v-S_v at* $0^o, 7.5^o$ *and* 15^o *for two sets of identical, vertical, gas-filled fractures with different alignments and the inter-fracture angle varying from* $0 - 90^o$ *(with the angle-bisector along* 90^o *azimuth) in 10 equal steps, as indicated by the arrows; d=0.001,* $\eta_c = 0.05$ *for each set.*

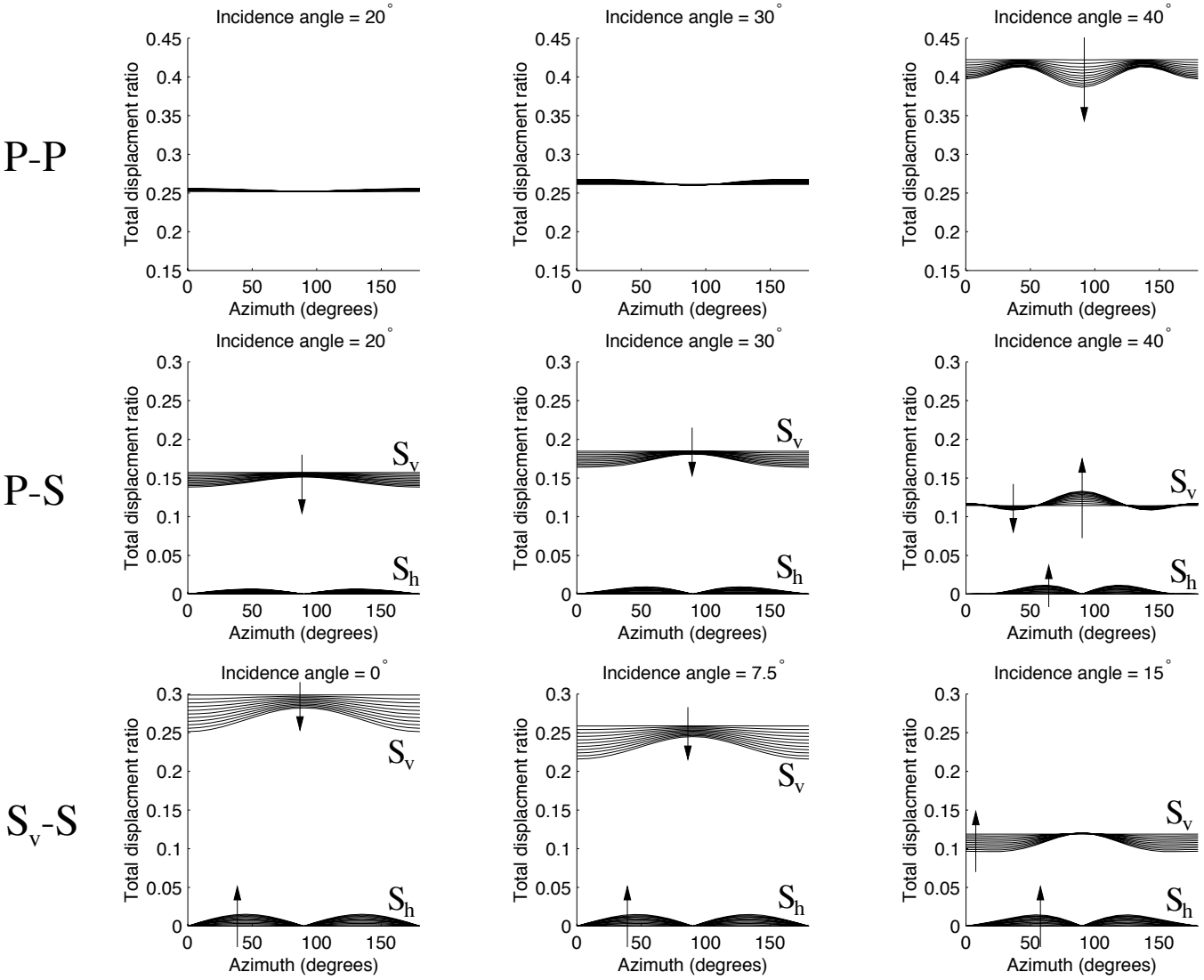

Figure 17: *P-P and P-S_v AVAz for for two sets of vertical, brine-filled fractures with one set of aligned along* 60^o *and the second along* 120^o *and varying crack density of both sets. AVAz curves for P-P and P-S_v reflections at* $20^o, 30^o$ *and* 40^o *incidence and for S_v-S_v at* $0^o, 7.5^o$ *and* 15^o *for two sets of vertical, brine-filled fractures with one set of aligned along* 60^o *and the second along* 120^o*; η_c for both sets varies from 0.00005-0.075, as indicated by the arrows and d =0.001.*

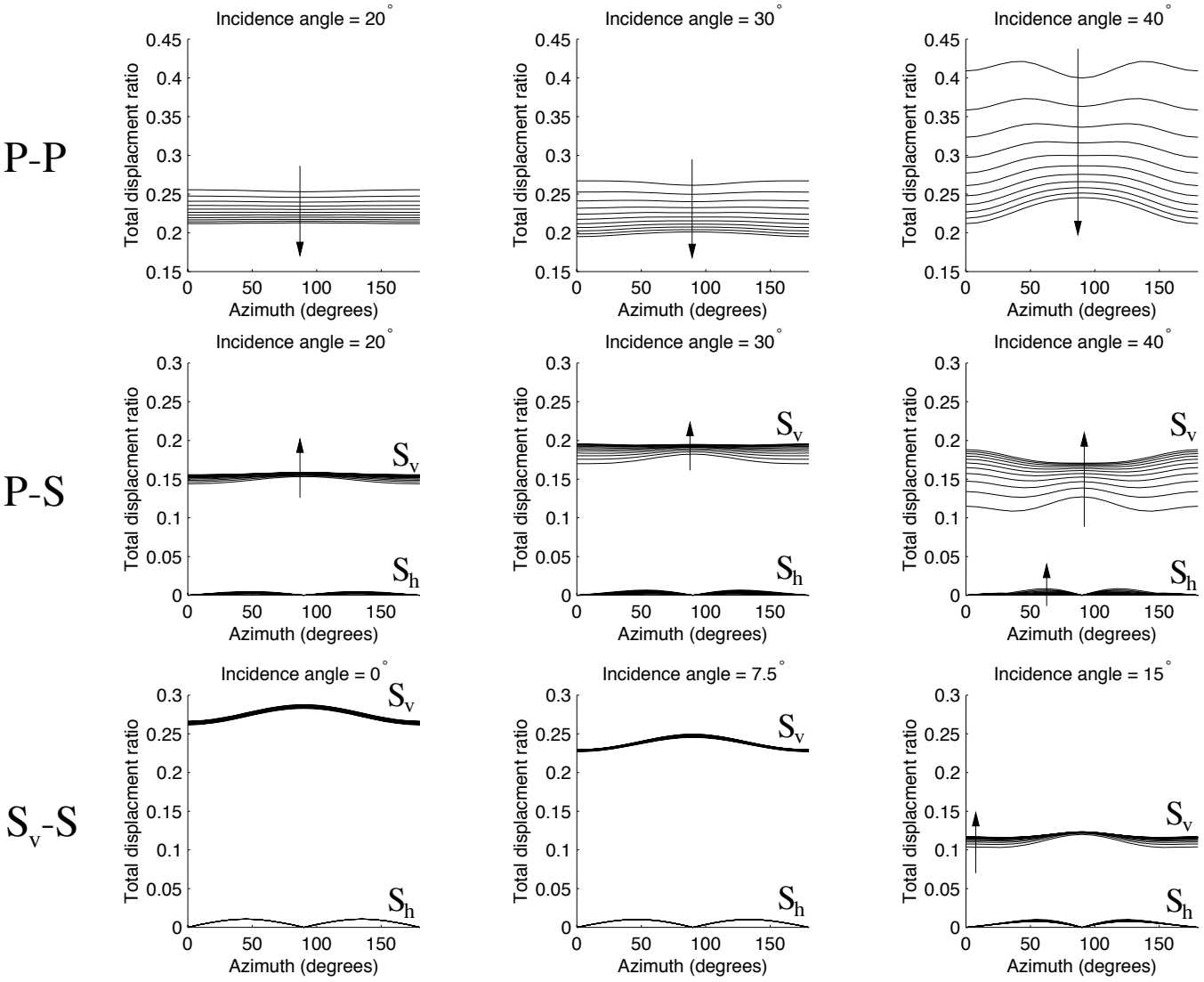

Figure 18: *P-P and P-S_v AVAz for for two sets of vertical, brine-filled fractures with one set of aligned along* 60^o *and the second along* 120^o *and varying aspect ratio of both sets. AVAz curves for P-P and P-S_v reflections at* $20^o, 30^o$ *and* 40^o *incidence and for S_v-S_v at* $0^o, 7.5^o$ *and* 15^o *for two sets of vertical, brine-filled fractures with one set of aligned along* 60^o *and the second along* 120^o*; aspect ratio for both sets varies from 0.0001-0.1, as indicated by the arrows and* $\eta_c = 0.05$.

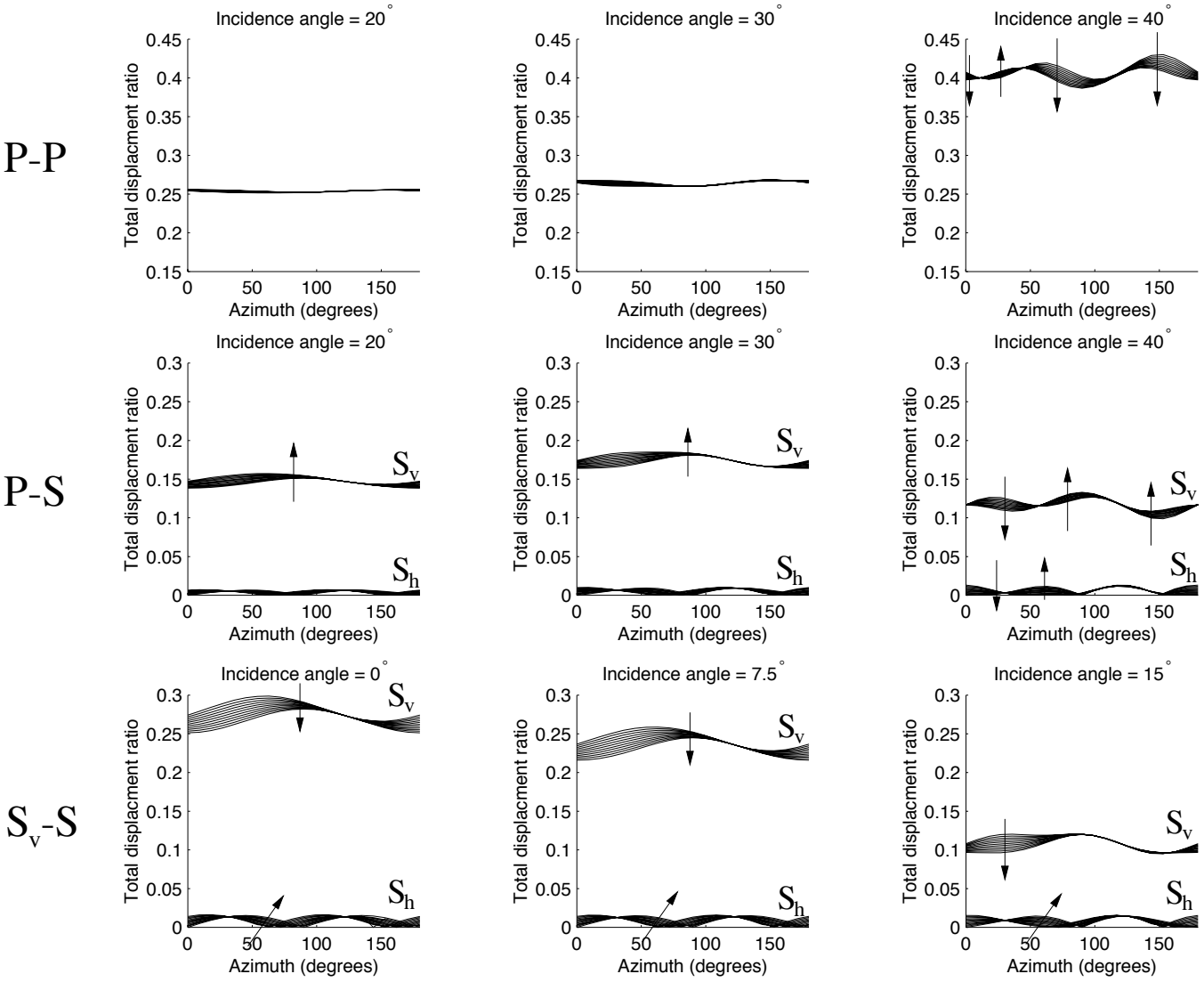

Figure 19: *P-P and P-S_v AVAz for for two sets of vertical, brine-filled fractures with one set of aligned along* 60^o *and the second along* 120^o *and varying crack density of one sets. AVAz curves for P-P and P-S_v reflections at* $20^o, 30^o$ *and* 40^o *incidence and for S_v-S_v at* $0^o, 7.5^o$ *and* 15^o *for two sets of vertical, brine-filled fractures with one set of aligned along* 60^o *and the second along* 120^o *azimuth; η_c for the fractures with strike=*120^o *varies from 0.00005-0.075, as indicated by the arrows, for the fractures with strike=*60^o $\eta_c = 0.075$ *and d=0.001 for both sets.*

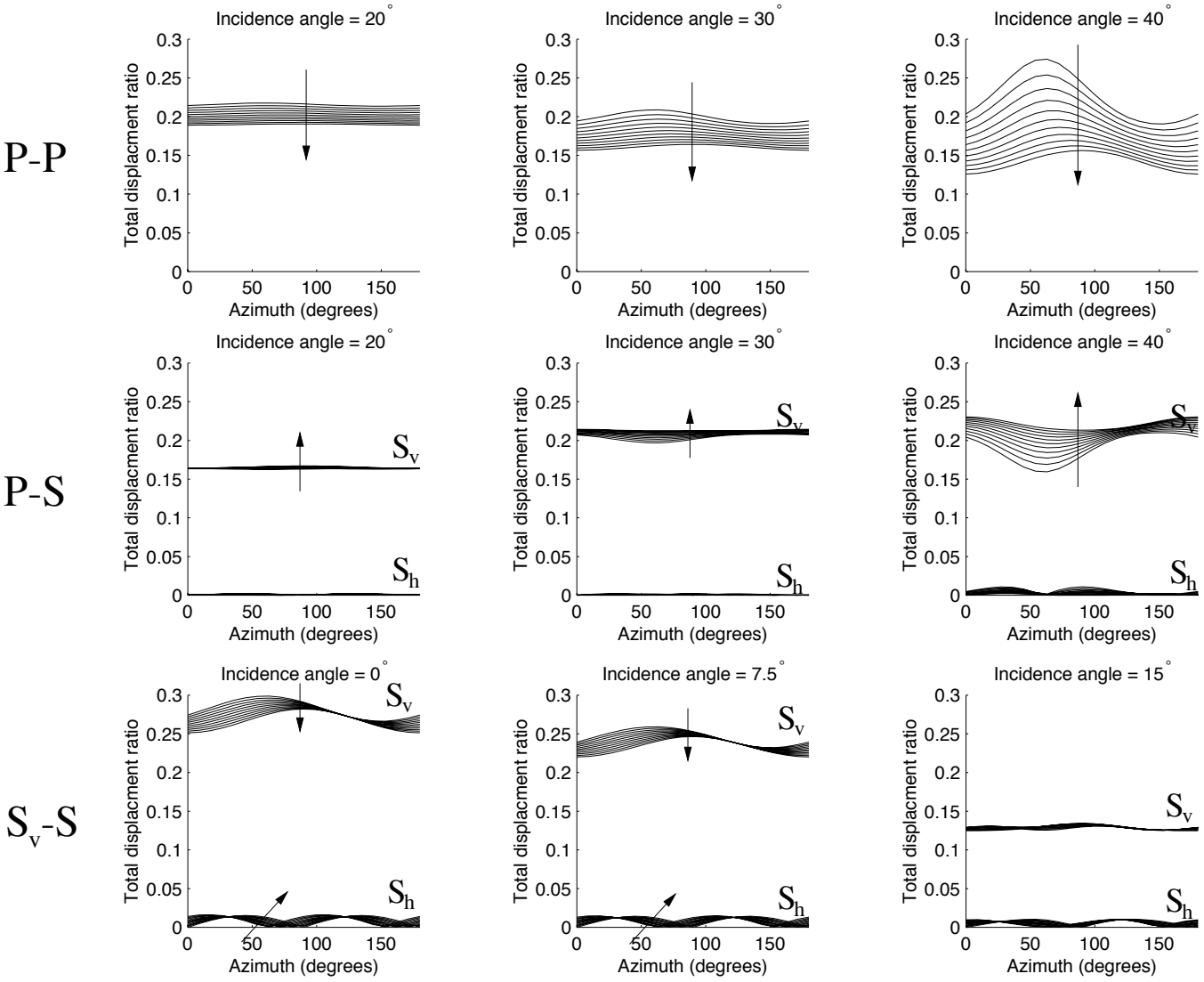

Figure 20: *P-P and P-S_v AVAz for for two sets of vertical, gas-filled fractures with one set of aligned along* 60^o *and the second along* 120^o *and varying aspect ratio of one sets. AVAz curves for P-P and P-S_v reflections at* $20^o, 30^o$ *and* 40^o *incidence and for S_v-S_v at* $0^o, 7.5^o$ *and* 15^o *for two sets of vertical, gas-filled fractures with one set of aligned along* 60^o *and the second along* 120^o *azimuth; η_c for the fractures with strike=*120^o *varies from 0.00005-0.075, as indicated by the arrows, for the fractures with strike=*60^o $\eta_c = 0.075$ *and d=0.001 for both sets.*

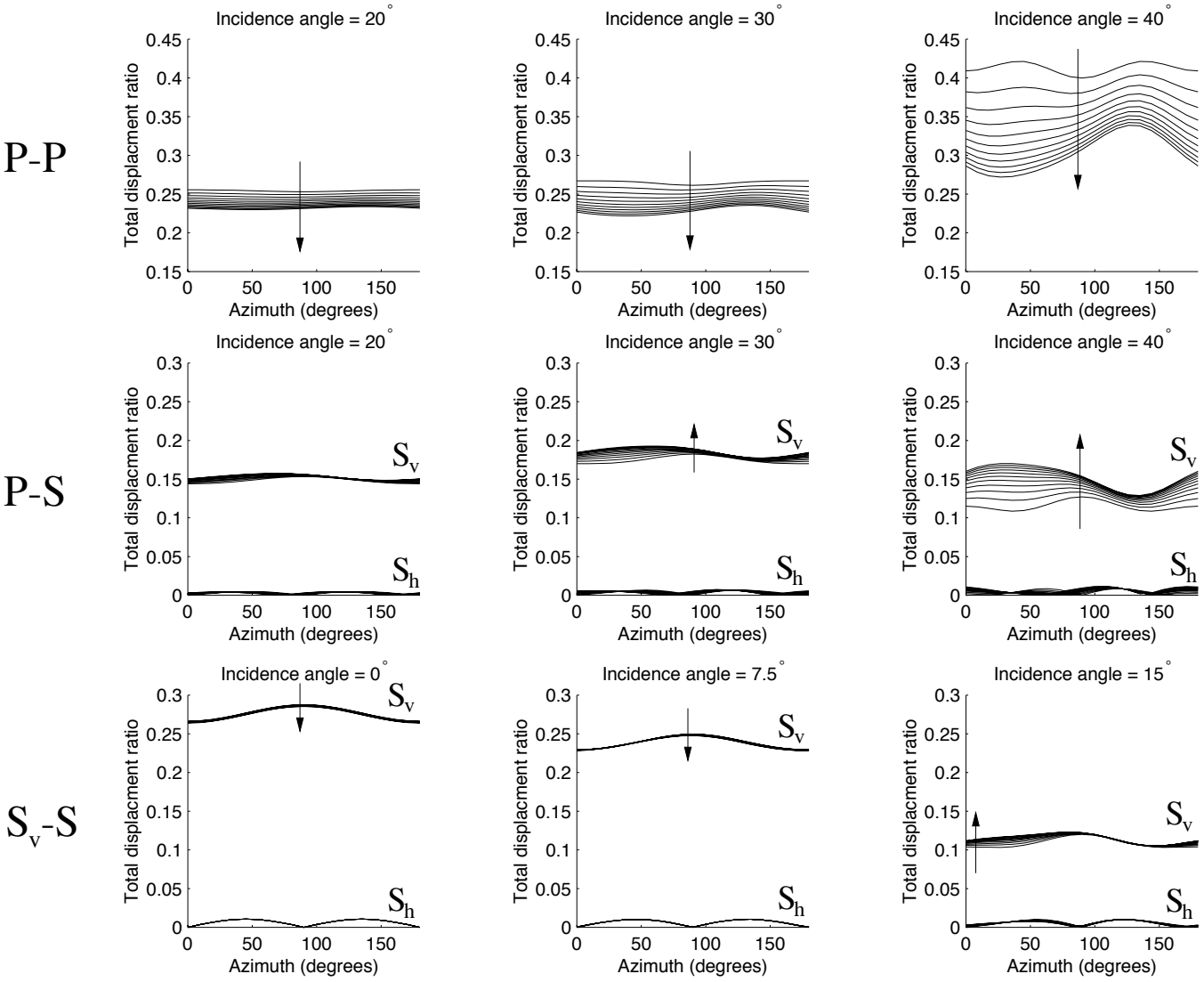

Figure 21: *P-P and P-S_v AVAz for for two sets of vertical, brine-filled fractures with one set of aligned along* 60^o *and the second along* 120^o *and varying aspect ratio of one sets. AVAz curves for P-P and P-S_v reflections at* $20^o, 30^o$ *and* 40^o *incidence and for S_v-S_v at* $0^o, 7.5^o$ *and* 15^o *for two sets of vertical, brine-filled fractures with one set of aligned along* 60^o *and the second along* 120^o *azimuth; aspect ratio for the fractures with strike=*120^o *varies from 0.0001-0.1, as indicated by the arrows, for the fractures with strike=*60^o *d=0.0001 and* $\eta_c = 0.05$ *for both sets.*

Appendix A:
Thomsen parameters for fractured HTI media

Here the Thomsen (1995) notation for fractured media used in the main text is explained with a minor redefinition to account for a change in coordinates. Thomsen (1995) re-casts the commonly used Thomsen (1986) parameters, ϵ, γ and δ, for the case of a small crack density of low-aspect-ratio fractures aligned with normals along the x_3 axis. This is achieved through a linearisation, with respect to crack density, of the results of Hoenig (1978) for penny-shaped cracks. This method places the cracks in a matrix containing *equant porosity* (additional smaller-scale porosity which will not cause any anisotropy in the system) and thus allows for the effect of fluid flow from the fractures to the matrix porosity. Small amounts of equant porosity ($< 10\%$) may be modelled as a dilute random distribution of spherical pores (Thomsen, 1995). Using this characterisation of the equant pore space Thomsen (1995) employs the results of Budiansky and O'Connell (1980) to define the *fluid influence factor*, D_{cp}. The Thomsen (1995) parameters are given below in terms of the stiffness, C_{ij}, and with respect to fracture properties but with a rotation so that the symmetry axis is in the horizontal, x_1, direction (the superscript *r* is therefore used to indicate rotated parameters are being used). Thus, for an HTI fractured medium,

$$\epsilon^r = \frac{C_{33} - C_{11}}{2C_{11}} = \left(\frac{8}{3}\right)\left(1 - \frac{K_f}{K_b}\right) D_{cp}\eta_c, \tag{A.1}$$

$$\gamma^r = \frac{C_{44} - C_{66}}{2C_{66}} = \left(\frac{8}{3}\right)\left(\frac{1-\nu_b}{2-\nu_b}\right)\eta_c, \tag{A.2}$$

$$\begin{aligned}\delta^r &= \frac{(C_{13}+C_{66})^2 - (C_{11}-C_{66})^2}{2C_{11}(C_{11}-C_{66})} \\ &= \frac{16}{3}\left[\left(1 - \frac{K_f}{K_b}\right)(1-\nu_b)D_{cp} - \left(\frac{1-2\nu_b}{2-\nu_b}\right)\right]\eta_c,\end{aligned} \tag{A.3}$$

where ν_b is the Poisson's ratio of the solid matrix, whilst K_b and K_f are the bulk moduli of the solid matrix and the fracture material respectively. With small amounts of equant porosity ($< 10\%$) the *fluid influence parameter*, D_{cp}, is (Thomsen, 1995),

$$D_{cp} = \left[1 - \frac{K_f}{K_b} + \frac{K_f}{K_b(\phi_p + \phi_c)}(A_p(\nu_b)\phi_p + A_c(\nu_b)\eta_c)\right]^{-1}, \tag{A.4}$$

where $\phi_c = \frac{4}{3}\eta_c\pi d$ is the fracture porosity (for crack density, η_c, and aspect ratio, *d*), ϕ_p is the (equant) matrix porosity, $A_c(\nu_b) = \frac{16(1-\nu_b^2)}{9(1-2\nu_b)}$ and $A_p(\nu_b) = \frac{3(1-\nu_b)}{2(1-2\nu_b)}$. This approach is relevant for moderately-high frequencies such that squirt-flow has an influence on the fracture-response but not so high that the time-scale of the passage of a seismic wave is too short for fluid movement. The formulation of this approach maintains a simplicity so that application within the EFFEC approach, described below, (to allow for hydraulic connectivity) is straight forward.

Appendix B:
Effec modelling

This appendix briefly outlines the effective medium approach used to determine the effective elasticity of fractured media employed in the numerical modelling of the main text. This approach (from Hall, 2000) is based on the generalised theory described by Schoenberg and Sayers (1995) extended to allow quantification of the additional fracture compliance terms.

In general, a fracture can be considered to be a poorly bonded interface which may have points of contact along its length and contains material that is different and, for the fractures of interest here, weaker in comparison to the surrounding media. In the presence of an applied stress there will be a difference in the displacements of the fracture surfaces to produce a displacement discontinuity, $[u_i]$, which is proportional to the tractions, t_i, on each fracture surface, *S*, with normal n_j. These tractions are related to the average stress in the medium, $\overline{\sigma}_{ij}$, by,

$$t_i = \overline{\sigma}_{ij} n_j, \tag{B.1}$$

and therefore the displacement discontinuity due to a single fracture may be described as,

$$\int_S [u_i] dS \propto \overline{\sigma}_{ij} n_j. \tag{B.2}$$

The sum of all the displacement discontinuities in a volume, *V*, produces an additional strain in the medium such that stress-strain relationship is (Schoenberg and Sayers, 1995),

$$\epsilon_{ij} = s_{ijkl_b} \overline{\sigma}_{kl} + \frac{1}{2V} \sum_r \int_{S_r} ([u_i] n_j + [u_j] n_i) dS. \tag{B.3}$$

Here s_{ijkl_b} is the compliance of the unfractured background medium and the second part of the equation represents the additional strain due to the presence of *r* displacement discontinuities (in this case fractures). This additional strain may be related to the applied stress, which is assumed to be continuous across the medium, through a 3x3 fracture system compliance tensor, Z_{ij} (Schoenberg and Sayers, 1995),

$$\frac{1}{V} \sum_r \int_{S_r} [u_i] dS = Z_{ip} \overline{\sigma}_{pq} n_q. \tag{B.4}$$

Combining (B.3) and (B.4) an effective compliance tensor, s_{ijkl}, of a rock, with an unfractured background containing *m* (differently) aligned fracture sets each contributing an additional compliance s_{ijkl_f} may be defined,

$$s_{ijkl} = s_{ijkl_b} + \sum_m s^{(m)}_{ijkl_f}, \tag{B.5}$$

where,

$$s_{ijkl_f} = \frac{1}{4}\sum_m (Z_{ik}^{(m)} n_l^{(m)} n_j^{(m)} + Z_{jk}^{(m)} n_l^{(m)} n_i^{(m)} + Z_{il}^{(m)} n_k^{(m)} n_j^{(m)} + Z_{jl}^{(m)} n_k^{(m)} n_i^{(m)}). \tag{B.6}$$

This representation describes the excess compliance due to the most general form of low aspect ratio fracture sets. However, if the fractures are rotationally invariant about their normal axis and have no significant preferential slip direction the fracture system compliance tensor may be simplified. For such fractures Z_{ij} is reduced to three non-zero elements which are given by just two independent terms, Z_N and Z_T, the normal and tangential fracture compliances,

$$Z_{ij} = Z_N n_i n_j + Z_T(\delta_{ij} - n_i n_j), \tag{B.7}$$

where δ_{ij} is the Kronecker delta. The excess compliance due to a single set of rotationally invariant fractures, with fracture normals oriented parallel to the x_1 axis, is therefore (Schoenberg and Sayers, 1995),

$$S_{mn_f} = \begin{pmatrix} Z_N & 0 & 0 & 0 & 0 & 0 \\ 0 & 0 & 0 & 0 & 0 & 0 \\ 0 & 0 & 0 & 0 & 0 & 0 \\ 0 & 0 & 0 & 0 & 0 & 0 \\ 0 & 0 & 0 & 0 & Z_T & 0 \\ 0 & 0 & 0 & 0 & 0 & Z_T \end{pmatrix}. \tag{B.8}$$

Thus from equations (B.5)-(B.8) the elastic stiffness of a medium containing a single set of aligned fractures is given by,

$$C_{mn} = \begin{pmatrix} M_b(1-\delta_N) & \lambda_b(1-\delta_N) & \lambda_b(1-\delta_N) & 0 & 0 & 0 \\ \lambda_b(1-\delta_N) & M_b(1-r_b^2\delta_N) & \lambda_b(1-r_b\delta_N) & 0 & 0 & 0 \\ \lambda_b(1-\delta_N) & \lambda_b(1-r_b\delta_N) & M_b(1-r_b^2\delta_N) & 0 & 0 & 0 \\ 0 & 0 & 0 & \mu_b & 0 & 0 \\ 0 & 0 & 0 & 0 & \mu_b(1-\delta_T) & 0 \\ 0 & 0 & 0 & 0 & 0 & \mu_b(1-\delta_T) \end{pmatrix}, \tag{B.9}$$

where $M_b = \lambda_b + 2\mu_b$, $r_b = \frac{\lambda_b}{M_b} \equiv \frac{\nu_b}{1-\nu_b}$, $0 \leq \delta_T = \frac{Z_T\mu_b}{1+Z_T\mu_b} < 1$ and $0 \leq \delta_N = \frac{Z_N M_b}{1+Z_N M_b} < 1$ and assuming an isotropic background matrix with Lamé parameters λ_b and μ_b.

If the elastic properties of the isotropic matrix in a fractured medium are known then theoretically it will be possible to determine the excess compliance due to aligned fractures from seismic data. Thus Z_N and Z_T represent the smallest amount of information that may be determined uniquely from data about aligned fractures. To further characterise aligned fracturing or forward model the effective elasticity of a fractured medium it will be necessary to determine Z_N and Z_T from given rock and fracture properties.

One of the strengths of the above approach for modelling the effective elasticity of fractured media is its generality, such that few assumptions need be made about the nature of aligned fracturing. However, this can

also be a drawback. This general approach is extended (Hall, 2000) by drawing parallels with other fracture theories to create a hybrid scheme for describing the elasticity of fractures and fractured media. For the modeling presented in this work two approaches are used, one appealing to Hudson (1981) (EFFECH modelling) and the other to Thomsen (1995) (EFFECT modelling) to define the additional fracture compliance terms; these are briefly described below.

EFFECH Modelling

The approach of Hudson (1980; 1981; 1986) determines the scattering effect of a single crack using the discontinuity in displacement across the crack faces described by an average fracture parameter, $\overline{U}_{ij}$, similar to Z_{ij} above, such that,

$$\int_S [u_i] dS = \frac{a^3}{\mu} \overline{U}_{ij} \overline{\sigma}_{jk} n_k, \tag{B.10}$$

after Hudson et al. (1996). Comparing (B.10) and (B.4) the fracture compliance is given as,

$$Z_{ij} = \frac{\eta_c}{\mu_b} \overline{U}_{ij}, \tag{B.11}$$

where η_c is the crack density defined as Na^3/V where *N* is the number of cracks, *V* the total volume of the medium and *a* the radius of the cracks.

For rotationally invariant fractures $\overline{U}_{ij}$ can be reduced to two terms $\overline{U}_{11}$ and $\overline{U}_{33}$. From (B.11) these terms relate directly to Z_N and Z_T, respectively. Hudson (1981) and Crampin (1984) give $\overline{U}_{11}$ and $\overline{U}_{33}$ for the case of a single penny-shaped crack, containing a weak isotropic material (with Lamé parameters λ_f and μ_f),

$$\begin{aligned} \overline{U}_{11} &= \tfrac{4}{3} \tfrac{(\lambda_b + 2\mu_b)}{(\lambda_b + \mu_b)} \tfrac{1}{(1+K)}, \\ \overline{U}_{33} &= \tfrac{16}{3} \tfrac{(\lambda_b + 2\mu_b)}{(3\lambda_b + 4\mu_b)} \tfrac{1}{(1+M)}, \end{aligned} \tag{B.12}$$

where,

$$K = \frac{(K_f + \frac{4}{3}\mu_f)}{\pi d \mu_b} \frac{(\lambda_b + 2\mu_b)}{(\lambda_b + \mu_b)}, \quad M = \frac{4\mu_f}{\pi d \mu_b} \frac{(\lambda_b + 2\mu_b)}{(3\lambda_b + 4\mu_b)}, \tag{B.13}$$

K_f is the bulk modulus of the crack-fill such that $K_f = \lambda_f + \frac{2}{3}\mu_f$. Equations (B.12) and (B.13) can be written in terms of velocities of the isotropic rock matrix by simply replacing $\frac{(\lambda_b+2\mu_b)}{(\lambda_b+\mu_b)}$ by $\left(1 - \frac{\beta^2}{\alpha^2}\right)^{-1}$ and $\frac{(\lambda_b+2\mu_b)}{(3\lambda_b+4\mu_b)}$ by $\left(3 - 2\frac{\beta^2}{\alpha^2}\right)^{-1}$. Thus Z_N and Z_T can be determined for penny-shaped cracks using equations (B.11) to (B.13).

EFFECT modelling

The effect of having equant matrix porosity into which fluid may flow from fractures, thereby hydraulically connecting the fractures and pore space, may be included in the EFFEC modelling by appealing to the

Thomsen (1995) formulation outlined in Appendix A. Thus new definitions of the excess compliances for penny-shaped cracks in a permeable matrix can be derived by comparing (A.1)-(A.3) and (B.9) (Hall, 2000),

$$Z_N = 2\epsilon^r \frac{(1-\nu_b)^2}{1-2\nu_b} \frac{1}{\lambda_b + 2\mu_b}, \tag{B.14}$$

$$Z_T = \frac{2\gamma^r}{\mu_b}. \tag{B.15}$$